RESEARCH ARTICLE SUMMARY

NEUROIMMUNOLOGY

Multimodal control of dendritic cell functions by nociceptors

Pavel Hanč, Rodrigo J. Gonzalez, Irina B. Mazo, Yidi Wang, Talley Lambert, Gloria Ortiz, Evan W. Miller, Ulrich H. von Andrian*

INTRODUCTION: There is growing evidence that neuroimmune interactions regulate immune and inflammatory responses. In particular, nociceptors, the afferent neurons that transmit the sensation of pain or itch in response to noxious stimuli, modulate immune cell functions in the peripheral tissues that they innervate. One of the major nociceptor targets are dendritic cells (DCs), which orchestrate local inflammatory responses and control adaptive immunity. Although nociceptors have been shown to exert control over DCs in several pathophysiological settings, the molecular mechanisms underlying nociceptor–DC cross-talk and the full scope of nociceptor involvement in DC immunobiology remain to be established.

RATIONALE: To determine the communication framework between nociceptors and DCs, we established an in vitro coculture system for the two cell types that enabled us to interrogate bona fide nociceptor–DC interactions without the involvement of other cell types. We explored the impact of nociceptors on both activated and steady-state DCs and defined, at the molecular level, communication pathways that rely on either physical cell–cell contact or nociceptor-derived soluble mediators. Subsequently, we investigated whether key observations in our reductionist in vitro system were predictive of the nociceptor–DC dialogue in several in vivo scenarios.

RESULTS: We identified three molecularly distinct modalities of communication used by nociceptors to control DC functions in a context-dependent manner. First, through the production of the chemokine CCL2, nociceptors can attract DCs and regulate their tissue dwell time. Second, through the activation-induced release of the neuropeptide calcitonin gene–related peptide (CGRP), nociceptors induce a transcriptional program in DCs characterized by the expression of *Il1b* as well as multiple other genes important for pathogen resistance and sentinel functions, but no overt DC activation. Third, through direct electrical coupling, firing nociceptors trigger a Ca^{2+} flux and membrane depolarization in DCs and potentiate DC responses to inflammatory stimuli such as Toll-like receptor (TLR) agonists. Accordingly, in vivo activation of dermal nociceptors enhanced the sentinel phenotype of DCs in the absence of immune stimuli and amplified DC-dependent tissue inflammation in response to TLR agonists. Furthermore, conditional ablation of CCL2 in nociceptors compromised the ability of dermal DCs to amplify local inflammation in the skin and to initiate adaptive immune responses against skin-derived antigens.

CONCLUSION: The multiple communication modalities characterized here reveal how nociceptors and DCs form a neuroimmune unit that integrates the nociceptors' rapid responsiveness and finely honed ability to sense and respond to noxious stimuli with the DCs' ability to coordinate innate and adaptive immune responses. This merger of unique capabilities allows the nociceptor–DC unit to act as an advanced warning system. DCs in barrier tissues are therefore a priori primed to anticipate imminent pathogen encounter, respond more vigorously upon painful pathogen exposure, and fine-tune the subsequent orchestration of adaptive immune responses to peripheral antigens. ■

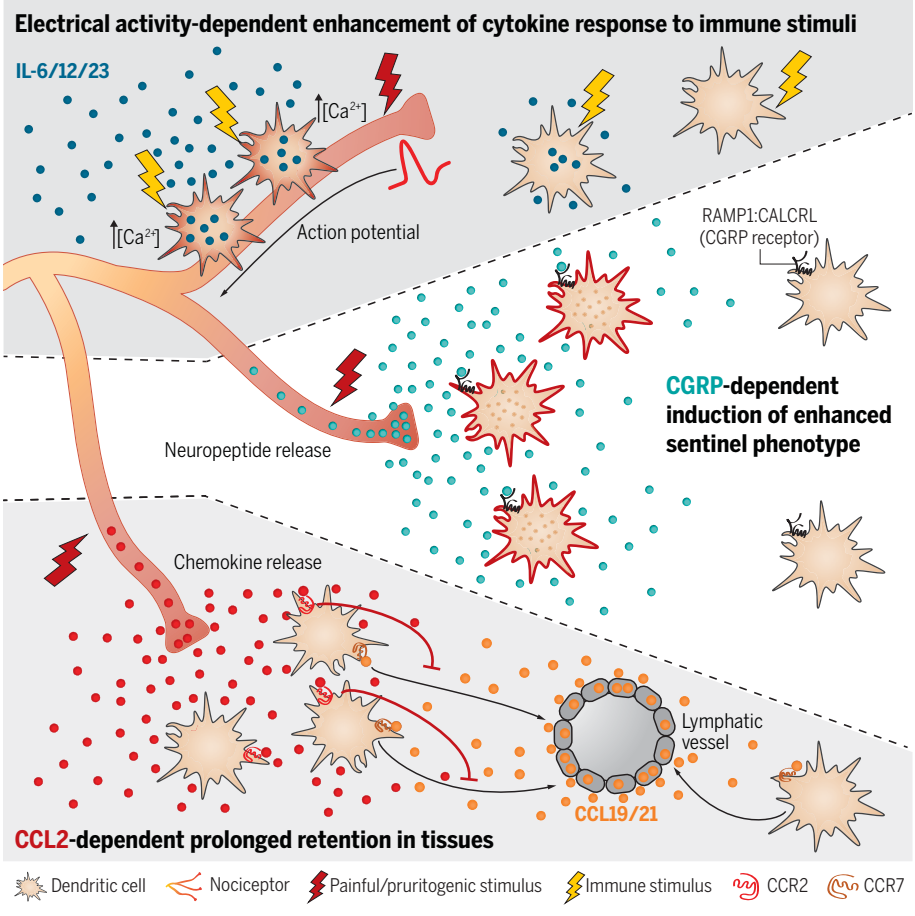

Nociceptors communicate with dendritic cells (DCs) using three distinct pathways to elicit context-dependent responses. (i) The release of CCL2 attracts DCs and regulates their dwell time within barrier tissues and antigen transport to lymph nodes; (ii) pain-induced release of the neuropeptide CGRP alters the transcriptional profile of steady-state DCs to assume enhanced sentinel functions; and (iii) when activated DCs contact firing nociceptors, the electrical activity amplifies their proinflammatory cytokine response. IL-6/12/23, interleukin-6, interleukin-12, interleukin-23.

The list of author affiliations is available in the full article online.
*Corresponding author. Email: uva@hms.harvard.edu
Cite this article as P. Hanč *et al.*, *Science* **379**, eabm5658 (2023). DOI: 10.1126/science.abm5658

READ THE FULL ARTICLE AT
https://doi.org/10.1126/science.abm5658

RESEARCH ARTICLE

NEUROIMMUNOLOGY

Multimodal control of dendritic cell functions by nociceptors

Pavel Hanč[1,2], Rodrigo J. Gonzalez[1,2], Irina B. Mazo[1,2], Yidi Wang[1,2], Talley Lambert[3], Gloria Ortiz[4], Evan W. Miller[4], Ulrich H. von Andrian[1,2]*

It is known that interactions between nociceptors and dendritic cells (DCs) can modulate immune responses in barrier tissues. However, our understanding of the underlying communication frameworks remains rudimentary. Here, we show that nociceptors control DCs in three molecularly distinct ways. First, nociceptors release the calcitonin gene–related peptide that imparts a distinct transcriptional profile on steady-state DCs characterized by expression of pro–interleukin-1β and other genes implicated in DC sentinel functions. Second, nociceptor activation induces contact-dependent calcium fluxes and membrane depolarization in DCs and enhances their production of proinflammatory cytokines when stimulated. Finally, nociceptor-derived chemokine CCL2 contributes to the orchestration of DC-dependent local inflammation and the induction of adaptive responses against skin-acquired antigens. Thus, the combined actions of nociceptor-derived chemokines, neuropeptides, and electrical activity fine-tune DC responses in barrier tissues.

Nociceptors are sensory neurons that respond to noxious stimuli by eliciting sensations of pain or itch and by modulating immune responses (*1*–*4*). Their somata reside in dorsal root ganglia (DRGs) with axons projecting to both the spinal cord and peripheral tissues (*5*). Nociceptors densely innervate barrier tissues (*6*) such as the skin and mucosal surfaces, which are also populated by dendritic cells (DCs). These sentinel leukocytes sense pathogen- and danger-associated molecular patterns and play critical roles in antigen presentation and control of adaptive immunity. Moreover, DCs coordinate local inflammation by secreting cytokines and other mediators (*7*). Intravital imaging demonstrated that dermal DCs congregate tightly around nociceptors, which profoundly affect DC functions (*8*–*10*). However, although these observations suggest direct cell–cell communication, the requirement for physical DC–nociceptor interactions versus a possible involvement of other intermediary cells has not been established. Furthermore, the role of nociceptor-derived neuropeptides in DC–nociceptor communication has been controversial, because neuropeptides appear dispensable in some experimental settings but exert either pro- or anti-inflammatory effects in other models (*8*, *9*, *11*).

[1]Department of Immunology, Harvard Medical School, Boston, MA 02115, USA. [2]The Ragon Institute of MGH, MIT, and Harvard, Cambridge, MA 02139, USA. [3]Cell Biology Microscopy Facility, Harvard Medical School, Boston, MA 02115, USA. [4]Departments of Chemistry, Molecular & Cell Biology, and Helen Wills Neuroscience Institute, University of California, Berkeley, CA 94720, USA.
*Corresponding author. Email: uva@hms.harvard.edu

Nociceptors potentiate cytokine responses by DCs in vitro

To address these outstanding questions, we cocultured primary DRG neurons and Flt3L-induced bone marrow DCs (BMDCs) (fig. S1A). Neuronal cultures contained >90% small-diameter NaV1.8$^+$ nociceptors (fig. S1B), whereas BMDC cultures comprised three major subsets: type 1 and 2 conventional DCs (cDCs) and plasmacytoid DCs (pDCs) (fig. S1C). Using this system, we examined DC responses to a Toll-like receptor 7 (TLR7) agonist, imiquimod (IMQ). Nociceptors did not affect DC maturation marker expression upon IMQ treatment (fig. S2A), but their presence significantly enhanced DC production of interleukin-12 (IL-12) p40, the shared subunit of IL-12 and IL-23 (Fig. 1A), as well as IL-6 (Fig. 1B). Conversely, production of another proinflammatory cytokine, tumor necrosis factor α (TNFα), was reduced (Fig. 1C). A likely mechanism for TNFα down-regulation is the action of calcitonin gene–related peptide (CGRP), a nociceptor-derived neuropeptide known to inhibit cytokine production by myeloid leukocytes (*11*). Indeed, olcegepant, a CGRP receptor antagonist, rescued TNFα production in DC–nociceptor cocultures, but had no impact on DCs alone (fig. S2B). Olcegepant did not affect DC production of IL-12 p40 or IL-6 regardless of whether nociceptors were present (fig. S2, C and D), indicating that this cytokine-promoting effect of nociceptors on DCs was CGRP independent. By contrast, a different myeloid cell type, BM-derived macrophages, showed decreased or unaltered cytokine responses to IMQ in nociceptor cocultures (Fig. 1D). Finally, coculture with hippocampal or cortical neurons did not alter DC responses to IMQ (Fig. 1E and fig. S2E). Thus, the potentiation of inflammatory cytokine production (other than TNFα) is a unique and specific consequence of the DC–nociceptor dialogue.

Numerous stimuli can trigger inflammatory cytokine production by DCs, including damage-associated molecular patterns (DAMPs) released from dead or distressed cells (*12*). A DC response to DAMPs from dead nociceptors could conceivably provide a trivial explanation for the exacerbated IMQ effect. However, DCs cocultured with nociceptors killed by prior fixation showed no enhanced cytokine production (Fig. 1F and fig. S2F). Moreover, treatment with lidocaine (a voltage-gated sodium channel blocker) and QX314 (a membrane-impermeable quaternary derivative of lidocaine), which together produce a long-lasting blockade of neuronal activity (*13*), dampened the ability of nociceptors to potentiate DC cytokine responses (Fig. 1G and fig. S2G). Thus, nociceptors must be alive and electrically active to exert their effects.

IMQ stimulated IL-12 p40 production in only a fraction of DCs, which increased in a concentration-dependent manner. Nociceptor cocultures increased the frequency of responding cDCs, but did not grossly alter the amount of cytokine detected per cell (Fig. 1H). By contrast, IMQ treatment of pDCs induced only a modest response, which was minimally affected by nociceptors (fig. S3A). Accordingly, the accumulation of interferon β (IFN-β), a prototypical pDC cytokine (*14*), was also unaffected by nociceptors (fig. S3B). Finally, although only cDC2s and pDCs produced IL-6 in response to IMQ (fig. S3C), the proportion of IL-6$^+$ cDC2s was significantly increased in the presence of nociceptors (fig. S3C), whereas pDCs in nociceptor cocultures showed only a weak, statistically nonsignificant trend toward increased IL-6 production (fig. S3C). Thus, cDCs, but not pDCs, are affected by nociceptors, at least under these experimental conditions, and the presence of electrically active nociceptors increases the proportion of DCs responding to a given dose of IMQ, presumably by decreasing the activation threshold to initiate cytokine production.

Cytokine potentiation requires concomitant activation of nociceptors and DCs

The principal IMQ receptor, TLR7 (*15*), is robustly expressed in murine DCs, but it has also been reported in sensory neurons (*16*). To clarify its role in this process, we established cocultures in which either nociceptors or DCs had been harvested from *Tlr7*$^{-/-}$ mice (*17*). Cytokine responses to IMQ were abrogated when DCs lacked TLR7, whereas *Tlr7*$^{-/-}$ and wild-type (WT) nociceptors equally enhanced cytokine production by WT DCs (Fig. 1I and

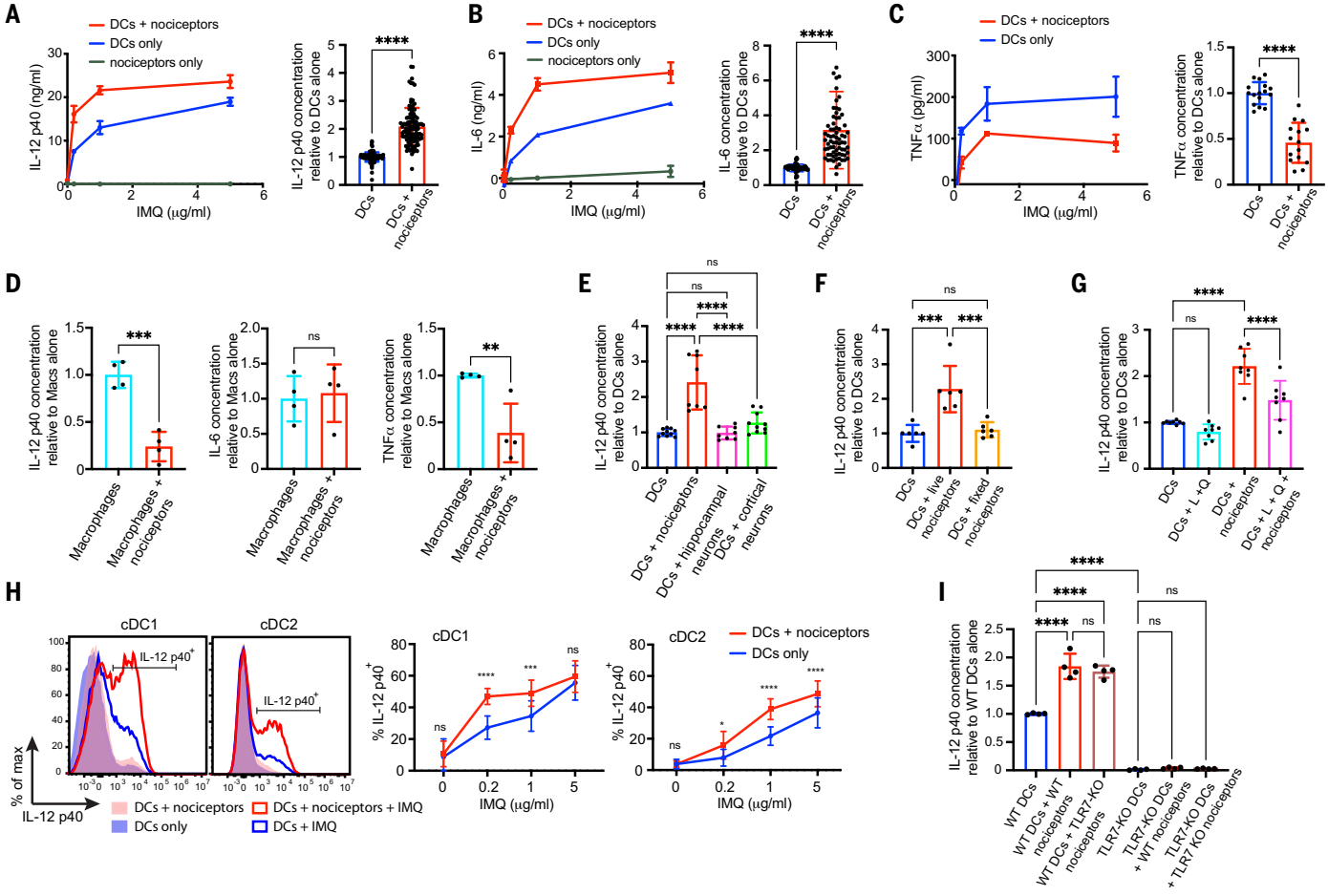

Fig. 1. Nociceptors enhance proinflammatory cytokine production by IMQ-activated DCs in vitro. BMDCs and nociceptors were cultured either separately or together and treated overnight with proinflammatory stimuli. Indicated cytokines were measured by ELISA in supernatants. (**A** to **C**) One representative dose response to IMQ (left panels) and summary of 42 (n = 104) (A), 37 (n = 74) (B), and 7 (n = 16) (C) experiments (right panels) for 1 μg/ml IMQ. (**D**) BM-macrophages were cultured alone or in the presence of nociceptors and treated with 1 μg/ml IMQ overnight. Summary of two experiments (n = 4) is shown. (**E**) BMDCs were cocultured with nociceptors, cortical neurons, or hippocampal neurons and treated with 1 μg/ml IMQ overnight. Summary of three experiments (n = 6 to 10) is shown. (**F**) BMDCs were cocultured with live or fixed nociceptors and treated with 1 μg/ml IMQ. Summary of three experiments (n = 6) is shown. (**G**) DCs were cocultured with nociceptors and treated with lidocaine + QX314 and 1 μg/ml IMQ. Summary of four experiments (n = 8) is shown. (**H**) Intracellular content of IL-12 p40 in BMDCs left untreated (full histograms) or treated with IMQ (open histograms) in isolation or in a coculture with nociceptors was assessed using flow cytometry. One representative experiment (left) and quantitation of eight independent experiments (right; n = 16) are shown. (**I**) WT or *Tlr7*-knockout (KO) DCs were cocultured with WT or *Tlr7*-KO nociceptors and treated with 1 μg/ml IMQ. Summary of two (n = 4) experiments is shown. Across all panels, data represent mean ± SD. Unpaired t test [(A) to (D)], one-way ANOVA with Tukey's multiple-comparisons test (F), or two-way ANOVA with Tukey's multiple-comparisons test [(E) and (G) to (I)] were used for statistical analysis: $^*P < 0.05$, $^{**}P < 0.01$, $^{***}P < 0.001$, $^{****}P < 0.0001$.

fig. S4A). Thus, nociceptors cannot by themselves elicit a cytokine response in DCs unless DCs are directly stimulated. Nonetheless, concomitant IMQ stimulation of nociceptors was required, but independently of TLR7. IMQ can directly gate the cation channel TRPA1 (*18*, *19*), and a TRPA1 inhibitor prevented nociceptor enhancement of DC responses to IMQ (fig. S4B).

The fact that IMQ may act on both DCs and nociceptors although through different mechanisms prompted us to investigate other immune stimuli, including zymosan (a TLR2 and Dectin-1 agonist), polyinosinic:polycytidylic acid (poly-I:C) (a TLR3 agonist), lipopolysaccharide (LPS) (a TLR4 agonist), flagellin (a TLR5 agonist), or CpG (a TLR9 agonist). All of these agents activate DCs, but only LPS, flagellin, and zymosan stimulate nociceptors by direct gating of ion channels or through membrane receptors such as TLR4 or Dectin-1 (*20*–*22*). Accordingly, nociceptors potentiated DC cytokine responses to zymosan, LPS, and flagellin, but not to poly-I:C or CpG (Fig. 2A and fig. S4C). Finally, as expected, nociceptors potentiated the LPS response irrespective of TLR7 expression by DCs (fig. S4D), indicating that *Tlr7*$^{-/-}$ DCs did not respond to IMQ because of their inability to register the stimulus and not because of other inherent functional defects.

Next, to test whether nociceptors can also enhance DC cytokine responses to infectious microbes, we exposed nociceptor–DC cocultures to viral [influenza A virus (IAV)], bacterial (ultraviolet light–inactivated *Streptococcus pnneumoniae*), or fungal (*Candida albicans*) pathogens that are commonly encountered in barrier tissues. IL-12 p40 was induced by every tested pathogen, whereas IL-6 was only induced by *S. pneumoniae* and IAV. Regardless of the microbial challenge, coculture with nociceptors markedly enhanced these responses (Fig. 2B and fig. S4E), suggesting that the paradigm of nociceptor enhancement of DC cytokine production may

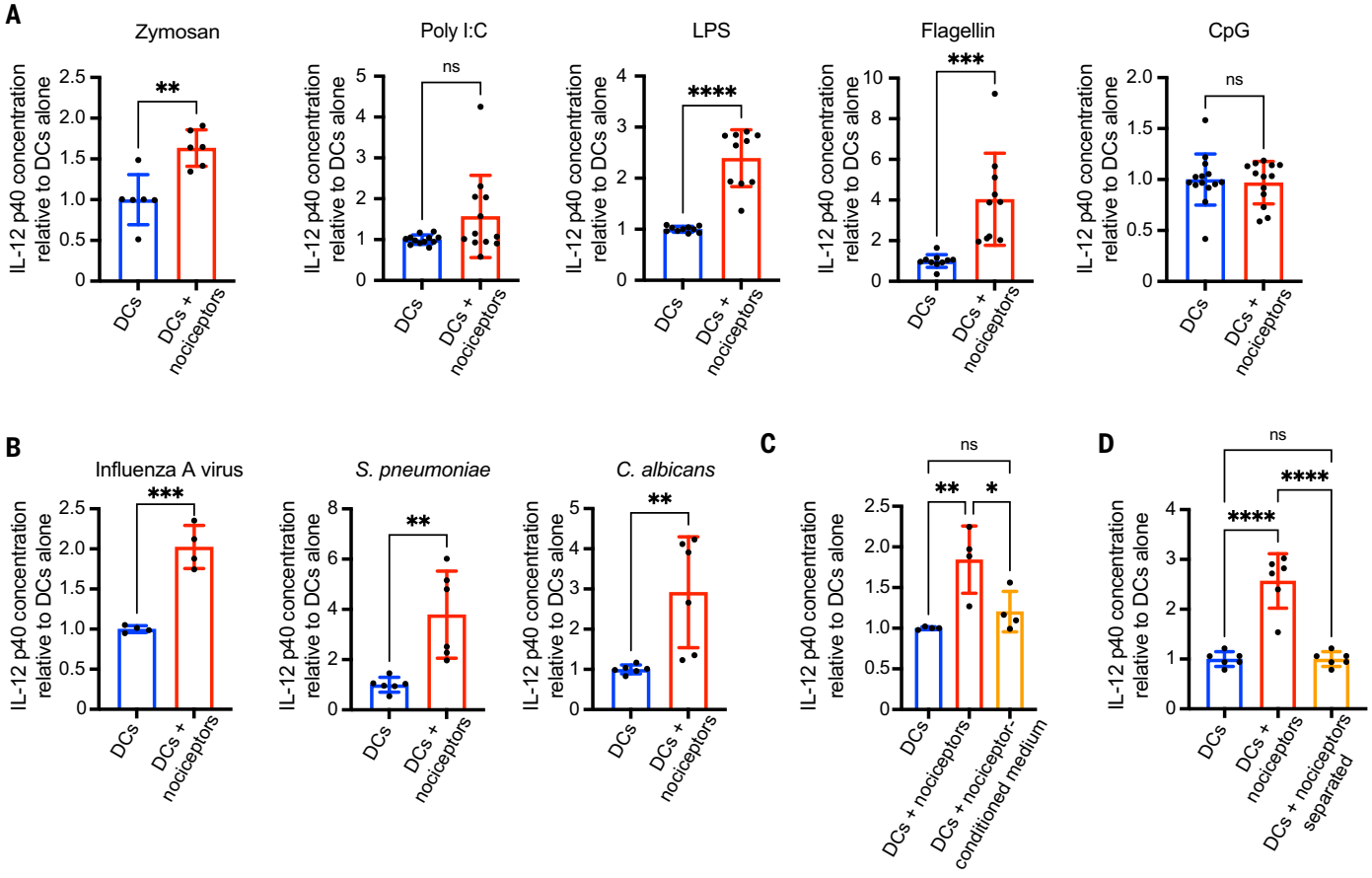

Fig. 2. Nociceptors enhance DC cytokine response to various stimuli in a contact-dependent manner. (**A** and **B**) BMDCs and nociceptors were either cultured separately or together and treated overnight with indicated nonmicrobial (A) or microbial (B) stimuli. Summary of two to five experiments (n = 4 to 12) is shown. (**C**) BMDCs were cultured alone, with nociceptors, or in a transferred medium in which nociceptors had been stimulated and treated with IMQ overnight. Summary of three experiments (n = 4) is shown. (**D**) BMDCs were cultured in Transwell plates either alone or with nociceptors in a manner that allowed or prevented direct physical contact between the cell types. Summary of three experiments (n = 6) is shown. IL-12 p40 concentration was measured by ELISA in supernatants. Across all panels, data represent mean ± SD. Unpaired t test [(A) and (B)] or one-way ANOVA with Tukey's multiple-comparisons test [(C) and (D)] were used for statistical analysis: *P < 0.05, **P < 0.01, ***P < 0.001, ****P < 0.0001.

apply to a host of inflammatory and infectious stimuli.

DC cytokine potentiation by nociceptors requires physical contact but not neuropeptides

Upon activation, nociceptors release immunomodulatory neuropeptides, particularly the CGRP-family of neuropeptides (CGRP, adrenomedullin, and intermedin) (*23*), substance P (SP) (*24*), vasoactive intestinal peptide (VIP) (*25*), and pituitary adenylate cyclase-activating peptide (PACAP) (*25*). However, DC exposure to neuropeptides did not enhance the IMQ-induced production of IL-12 p40 or IL-6, nor did neuropeptides induce de novo cytokine responses in unstimulated DCs (fig. S4F). Similarly, nociceptor-conditioned medium did not enhance cytokine production by IMQ-stimulated DCs, suggesting that direct cell–cell contact may be required (Fig. 2C and fig. S4G). Indeed, when DCs and nociceptors were separated by a filter membrane in a Transwell device that allowed diffusion of soluble molecules while preventing physical contact, DCs produced no more IL-12 p40 than did DCs cultured alone (Fig. 2D). Furthermore, the accumulation of IL-6 was decreased, albeit not quite to the levels observed in DC-only cultures (fig. S4H). Thus, the presence of electrically competent nociceptors enhances DC cytokine responses to multiple exogenous immune stimuli in a manner independent of neuropeptides and is dependent on physical contact or at least close physical proximity.

Nociceptors attract DCs by secreting CCL2

Seeing the importance of physical contact for nociceptor–DC communication in vitro, and in light of their close proximity in vivo (*9*, *10*), we investigated whether nociceptors produce DC chemoattractants. Indeed, all DC subsets migrated toward nociceptor-conditioned medium in a concentration-dependent manner (Fig. 3A and fig. S5, A and B). Using two multiplexed assays, we identified several known chemoattractants in nociceptor-conditioned medium, with CCL2 and chemerin being the most abundant (fig. S5, C and D). Although chemerin immunodepletion had no effect, CCL2 depletion significantly decreased DC migration toward nociceptor-conditioned medium (fig. S5E). Furthermore, medium conditioned by nociceptors from *Ccl2*$^{-/-}$ mice (*26*) showed a reduced capacity to attract DCs (Fig. 3A and fig. S5, A and B), indicating that CCL2 is the predominant DC chemoattractant secreted by nociceptors. Accordingly, CCL2 was detectable in medium conditioned by WT but not *Ccl2*$^{-/-}$ nociceptors (fig. S5F) and increased after nociceptor stimulation with capsaicin or IMQ (fig. S5G). A previous report linked CCL2 up-regulation in nociceptors to activation of

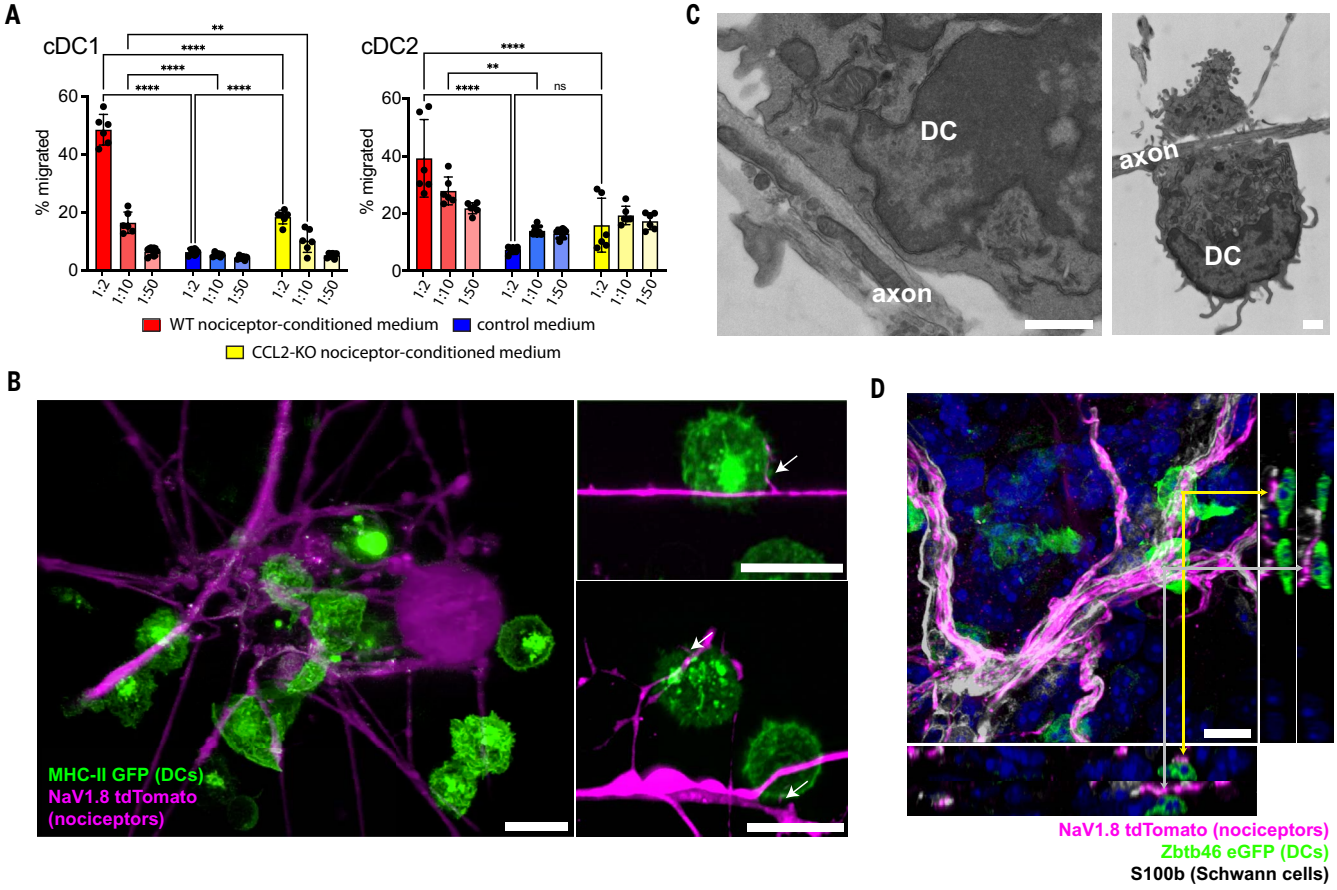

Fig. 3. Nociceptors attract and physically interact with DCs in vitro. (**A**) Migration of BMDCs toward WT nociceptor-conditioned, control, and *Ccl2*$^{-/-}$ nociceptor-conditioned medium was assessed in a Transwell chemotaxis assay (5-μm pore size). Summary of three experiments (n = 6) is shown. Data represent mean ± SD. Two-way ANOVA with Tukey's multiple-comparisons test was used for statistical analysis: *P < 0.05, **P < 0.01, ***P < 0.001, ****P < 0.0001. (**B**) DCs from MHC-II eGFP mice were cocultured with nociceptors from NaV1.8$^{Cre/+}$ ROSA$^{tdTomato/+}$ donors and imaged using a lattice light-sheet microscope (see also movies S2 and S3). Arrowheads highlight some of the points of contact between nociceptors and DCs. Scale bars, 10 μM. (**C**) Transmission electron micrographs of a DC contacting a nociceptor axon. Two representatives of >10 similar images are shown. Scale bars, 1 μM. (**D**) Dermal sheets from BM chimeric animals expressing tdTomato under the NaV1.8 promoter in somatic cells and eGFP under the Zbtb46 promoter in the hematopoietic lineage were stained with anti-S100 antibody to identify Schwann cells and analyzed using confocal microscopy.

MyD88, a signaling adaptor critical for TLR function (*27*). Indeed, LPS-induced ligation of TLR4 resulted in markedly increased levels of CCL2 (fig. S5H). Moreover, in agreement with previous studies, unstimulated cDC1s and cDC2s expressed uniformly high levels of the CCL2 receptor CCR2, which was down-regulated upon LPS exposure, coincident with CCR7 up-regulation (fig. S5I) (*28*). In macrophages, CCL2 reportedly affects the secretion of cytokines including IL-12 (*29*). However, CCL2 had no effect on cytokine production by DCs, because *Ccl2*$^{-/-}$ and WT nociceptors potentiated the DC response to IMQ equally (fig. S5J).

DCs engage in tight and dynamic interactions with nociceptors

Next, using live-cell imaging, we observed that DCs engaged in tight and highly dynamic physical interactions with nociceptors (Fig. 3B, fig. S6A, and movies S1 to S3). Furthermore, transmission electron microscopy revealed a tight apposition of the plasma membranes of interacting cells (Fig. 3C). To determine whether similarly tight contacts occur in vivo, we transplanted BM from *Zbtb46*^{eGFP} (where eGFP is enhanced green fluorescent protein) donors (*30*) into irradiated *Scn10a*$^{Cre/+}$*Rosa26*$^{tdTomato/+}$ recipients. Nociceptors and DCs in these chimeras were identifiable by expression of tdTomato and GFP, respectively, and confocal microscopy analysis of dermal sheets revealed physical contacts between them (Fig. 3D).

Nociceptor activation induces calcium flux in interacting DCs

Given the importance of physical contact for effective communication between nociceptors and DCs and the observation that nociceptors attract DCs by the secretion of CCL2, we performed calcium imaging to assess whether and how signals propagate from activated neurons to interacting DCs. Upon treatment with the TRPV1 channel agonist capsaicin (*31*), a rapid increase in intracellular calcium occurred in both nociceptors and DCs (Fig. 4, A and B, and movie S4). Capsaicin did not elicit a calcium flux in DCs alone (Fig. 4B and movie S5), indicating that the capsaicin effect in cocultures was caused by the activation of nociceptors, not DCs.

To better approximate the anatomic relationship between DCs and nociceptors, we next used a culture device with two compartments connected by fluidically isolated microgrooves (*32*) (fig. S6B). Nociceptors plated in one compartment, the "neuronal compartment," sprouted axons across the microgrooves into the second compartment, the "DC compartment." Capsaicin stimulation of nociceptors in the neuronal compartment triggered axonal action potential propagation to the DC

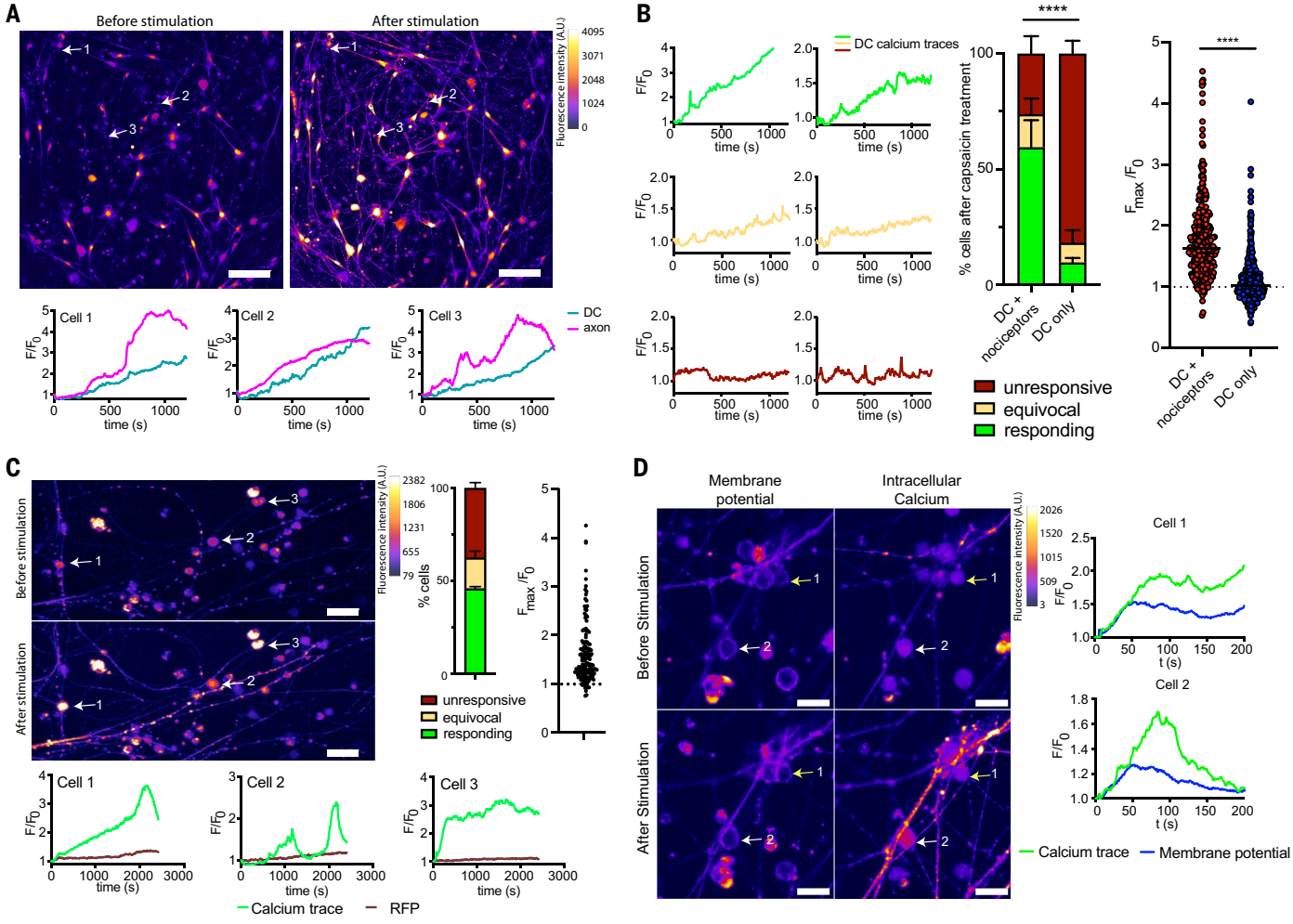

Fig. 4. Activation of nociceptors induces calcium mobilization and membrane depolarization in DCs. (**A**) Cells in nociceptor:DC cocultures were loaded with the calcium indicator dye Fluo-4 and imaged on a spinning disk confocal microscope. Left panel shows the culture before and right panel after the addition of capsaicin. Representative calcium traces of DCs and proximal axons (arrowheads) are shown in bottom panels (see also movies S4 and S5). (**B**) Calcium traces of representative responder (green), equivocal (yellow), and unresponsive (dark red) DCs (left panel) and quantification of four independent experiments as shown in (A), comparing the proportion of responder cells (middle panel) and the magnitude of calcium response in each cell (right panel). (**C**) Nociceptors were plated in one compartment (neuronal compartment) of a microfluidic device consisting of two wells that were separated by fluidically-isolated microgrooves. Once neuronal axons had grown across the microgrooves, DCs were added to the second compartment (DC compartment). All cells were loaded with Fluo-4, and the DC compartment was imaged on a spinning disk confocal microscope after capsaicin addition to the neuronal compartment. Some of the responding DCs are highlighted, and their calcium traces are shown in the lower panels. One representative and a quantitation of three independent experiments are shown (see also movie S6). (**D**) Cells in a nociceptor–DC coculture were loaded with Fluo-4 and a membrane potential indicator dye (BeRST) and imaged on a spinning disk confocal microscope. Top panels show the culture before and bottom panels after the addition of capsaicin. Some of the responding DCs are highlighted, and their calcium and membrane potential traces are shown in the right panel. One representative of two experiments is shown (see also movie S10). Across all imaging panels, warmer colors represent higher intracellular calcium concentration except in (D), left panels, where they indicate lower membrane potential (depolarization).

compartment, where DCs interacting with firing axonal segments fluxed calcium (Fig. 4C and movie S6) comparably to conventional cocultures (fig. S6C). Although some DCs fluxed calcium in sync with contacting axons (fig. S6D and movie S7), calcium flux kinetics in the DC population as a whole were nonuniform (Fig. 4C and fig. S6E), a phenomenon likely attributable to the dynamic nature of interactions, asynchronous firing of different axons, nonhomogeneous distribution of TRPV-1 expression among nociceptors, and potentially also differences between DC subsets.

Nociceptor activation induces membrane depolarization in interacting DCs

Neuronal calcium influx is triggered by membrane depolarization as action potentials propagate along axons. Therefore, we wondered whether the calcium flux in DCs was also accompanied by membrane depolarization. Indeed, using a ratiometric fluorescent probe, Di-8-ANNEPS, capsaicin-induced membrane depolarization was detected in both cell types in DC–nociceptor cocultures. Capsaicin, however, had no effect on DCs alone (fig. S6F and movies S8 and S9). Similarly, DCs and nociceptors stained with BeRST, a voltage-sensitive dye compatible with calcium imaging (*33*), depolarized and fluxed calcium in response to capsaicin (Fig. 4D and movie S10).

Thus, nociceptors attract DCs by producing CCL2 and engage in tight physical interactions,

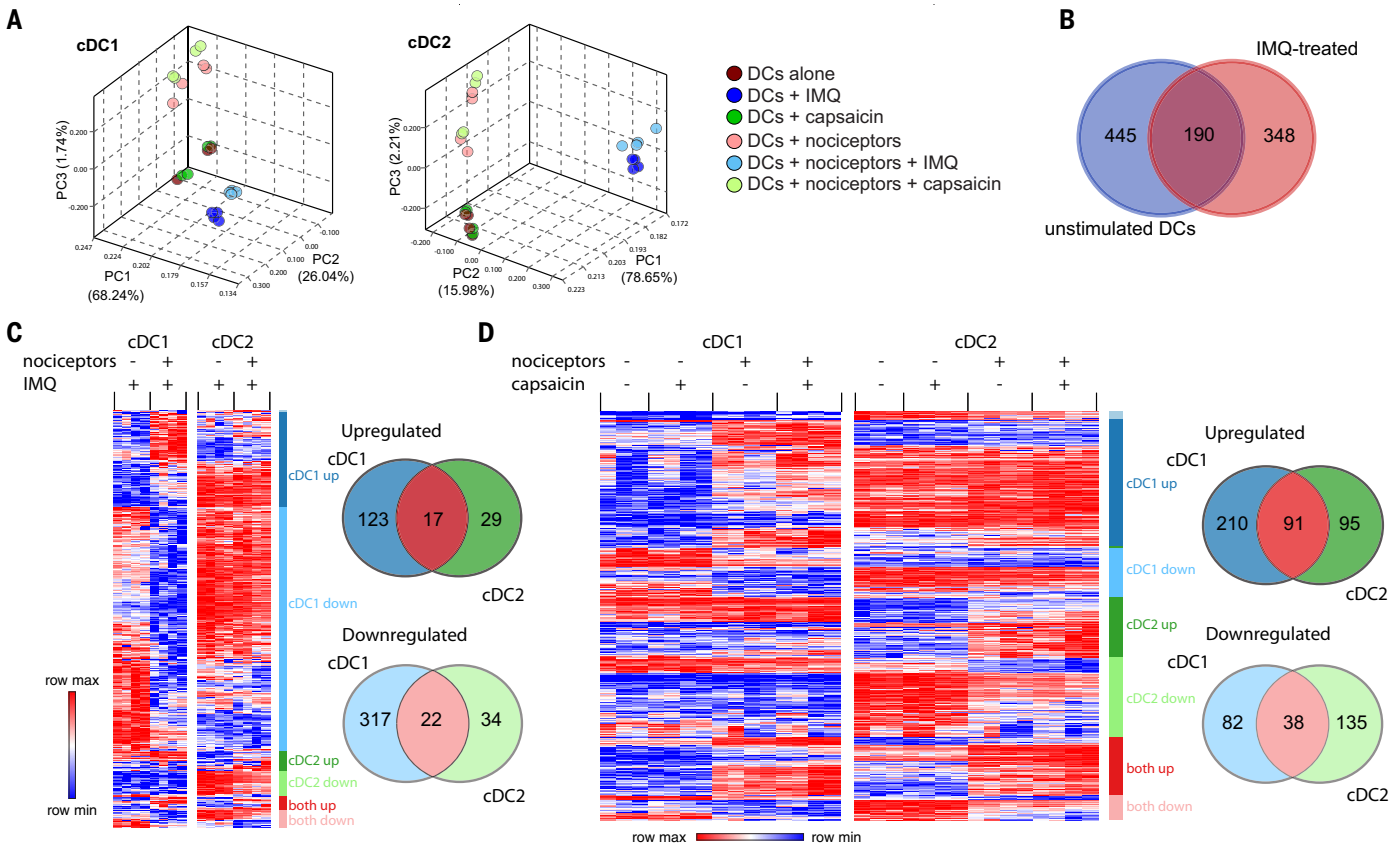

Fig. 5. Nociceptors modulate the DC transcriptome. (**A**) PCA of RNA-seq data from DCs treated with IMQ or capsaicin in the presence or absence of nociceptors. (**B**) Venn diagram of differentially regulated genes across DC subsets in coculture with nociceptors compared with DC monoculture. (**C** and **D**) Heatmap of genes differentially regulated (FC ≥ 2, FDR = 0.1) between DCs stimulated with IMQ in monoculture and in coculture with nociceptors (C) or DCs left untreated or treated with capsaicin in the presence or absence of nociceptors (D). Colored bars and sections of the Venn diagrams designate gene sets that are uniquely differentially regulated in cDC1s (blue), cDC2s (green), or co-regulated in the two subsets (red). Darker shades correspond to up-regulated genes and lighter shades to down-regulated genes.

presumably mediated by a yet-to-be-identified adhesion molecule(s). Electrical nociceptor activity induces in interacting DCs membrane depolarization and calcium influx, which may modulate myeloid cell functions (*34*, *35*). Indeed, calcium mobilization has been shown to increase IL-12 production by DCs upon TLR stimulation (*36*). Accordingly, coadministration of a calcium ionophore boosted the DC response to IMQ (fig. S7, A and B), analogous to our observations in nociceptor–DC cocultures.

Nociceptors induce transcriptomic changes in DCs

Next, to assess the impact of nociceptors beyond amplifying DC cytokine responses, we performed RNA sequencing (RNA-seq) on DCs cultured in the presence or absence of nociceptors and with or without IMQ or capsaicin. Principal components analysis (PCA) revealed that the mere presence of nociceptors induced profound transcriptomic changes in both resting and IMQ-treated cDCs (Fig. 5A). Further marginal changes observable in PCA space were induced by capsaicin stimulation of cocultures, whereas isolated DCs showed altered gene expression profiles only after exposure to IMQ, but not capsaicin. Across all conditions, 983 genes in cDCs were differentially regulated by nociceptors with a fold change (FC) ≥ 2 [false discovery rate (FDR) = 0.1]. Of the differentially regulated genes, a minority (190 genes) were shared between the IMQ-treated and -untreated groups, indicative of two largely independently regulated genesets, one modulated by nociceptors in immature DCs (445 genes) and a second that only became apparent upon DC activation (348 genes) (Fig. 5, B to D, and fig. S8A). Compared with cocultures with unstimulated nociceptors, capsaicin exposure resulted in only 16 differentially regulated genes in cDCs (FC ≥ 2; FDR = 0.1) (fig. S8B), suggesting that nociceptors express the most relevant communication molecule(s) constitutively, at least in vitro. Finally, consistent with our earlier observations (fig. S3, A to C), the presence of nociceptors exerted minimal effects on pDCs, in which only 38 genes were differentially expressed across all conditions (fig. S8, C and D).

Of the differentially regulated genes in IMQ-activated cDCs, most were selectively regulated in cDC1s, with a minority shared or unique to cDC2s (Fig. 5C). Gene-set enrichment analysis (GSEA) (*37*, *38*) revealed that among the hallmark gene sets (*39*), the most prominently up-regulated pathways in activated cDCs exposed to nociceptors were the glycolysis and hypoxia response pathways (fig. S9, A to C). This was consistent with the increased proportion of cytokine-producing cells (Fig. 1H and fig. S3C), because these two gene sets correlate with DC activation status (*40*). Additionally, GSEA revealed a down-regulation in the unfolded protein response and apoptotic signaling in activated cDC1s, suggesting that nociceptors may improve activated cDC1 survival. Most of the differentially regulated genes in immature cDCs (Fig. 5D) were likewise regulated in a subset-specific manner. However, the number of genes was comparable between cDC subsets, and more genes were co-regulated. These

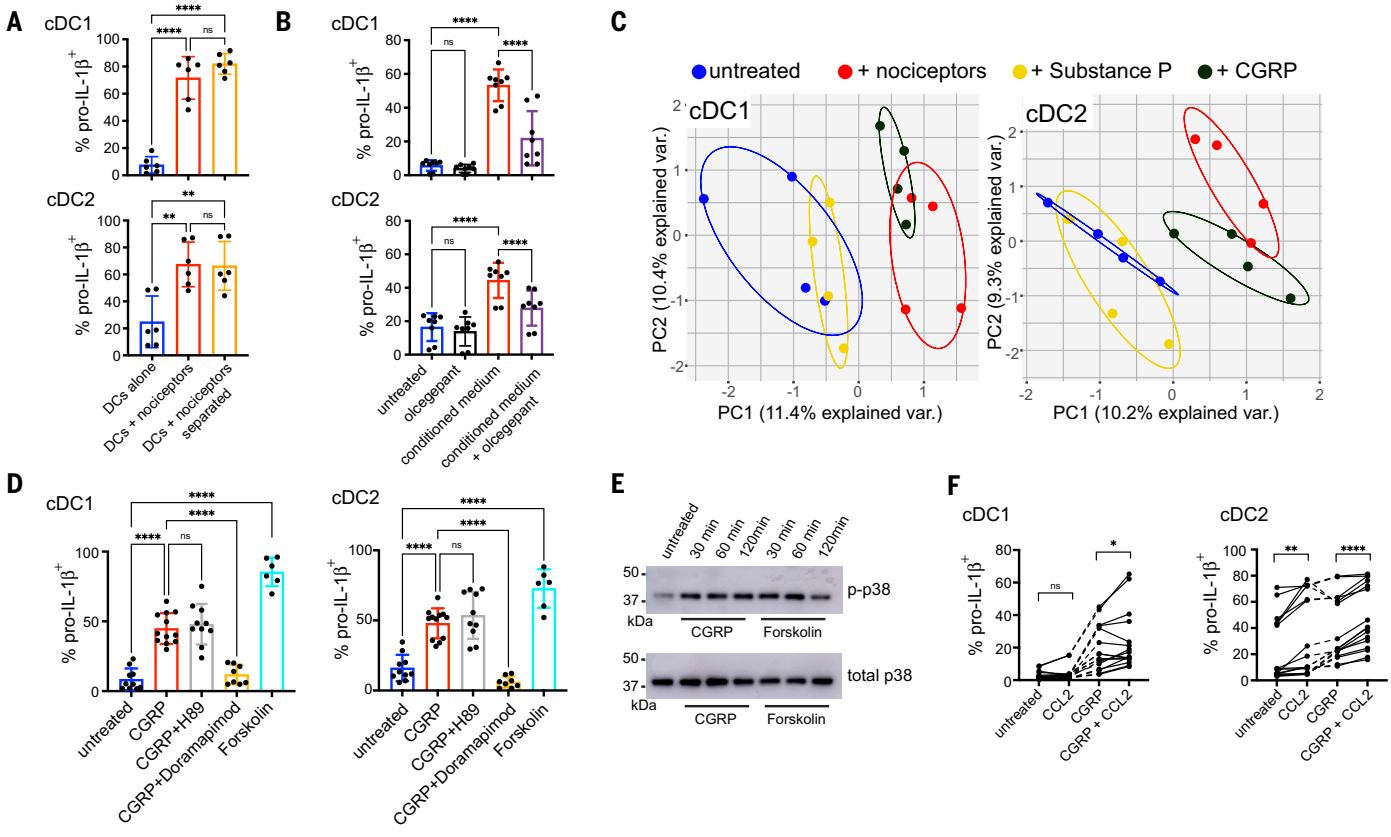

Fig. 6. CGRP induces an enhanced sentinel phenotype in DCs. (**A** and **B**) The intracellular content of pro–IL-1β was determined by flow cytometry in DCs that were directly cocultured with nociceptors, shared medium with nociceptors, or cultured alone (A) and in DCs that were incubated with nociceptor-conditioned medium in the presence or absence of CGRP receptor antagonist (olcegepant) (B). Summary of three to four independent experiments (n = 6 to 8) is shown. (**C**) PCA of RNA-seq data from DCs cultured alone, cocultured with nociceptors, or treated with CGRP or substance P. (**D**) DCs were treated with CGRP, CGRP + dorapamimod (p38 inhibitor), CGRP + H89 (PKA inhibitor), or forskolin (AC activator) overnight. The expression of pro–IL-1β was determined by flow cytometry. Summary of three to six experiments per condition is shown (n = 6 to 12). (**E**) DCs were treated with CGRP or forskolin for the indicated periods of time and lysed. Phosphorylation status of p38 was assessed by phospho-Thr180/Tyr182–specific antibody in immunoblot analysis (top). Total p38 was used as a loading control (bottom). One representative of three independent experiments is shown. (**F**) DCs were plated in wells coated with CCL2 and treated with CGRP overnight. Pro–IL-1β up-regulation was assessed by flow cytometry. Summary of eight independent experiments (n = 16) is shown. Across all panels, data represent mean ± SD. One-way ANOVA with Tukey's multiple-comparisons test (A), two-way ANOVA with Tukey's multiple-comparisons test [(B) and (D)], or paired t test (F) were used for statistical analysis: *P < 0.05, **P < 0.01, ***P < 0.001, ****P < 0.0001.

subset-specific effects of nociceptors likely reflect the fact that cDC1s and cDC2s perform distinct roles in vivo. Nonetheless, the genes co-regulated by nociceptors in cDCs included a number of genes coding for proteins involved in cDC sentinel functions, including pro–IL-1β (fig. S9D and table S1).

CGRP induces an enhanced sentinel phenotype in DCs

Unlike many other proinflammatory cytokines, IL-1β is synthesized as a pro-protein (pro–IL-1β), which is proteolytically processed and released upon inflammasome activation (*41*). Consistent with the lack of overt DC activation in unstimulated cocultures, mature IL-1β was undetectable in coculture supernatants (fig. S10A). However, nociceptors induced a pronounced, contact-independent intracellular accumulation of pro–IL-1β in DCs (Fig. 6A), which was reproduced by exposure to nociceptor-conditioned medium (fig. S10B), suggesting the involvement of a soluble signal(s) such as a neuropeptide(s). Indeed, although SP, PACAP, and VIP were inactive, adrenomedullin and intermedin induced pro–IL-1β expression at submicromolar concentrations, and αCGRP was singularly potent even at picomolar concentrations (fig. S10C). Accordingly, CGRP was readily detectable in nociceptor-conditioned medium and further increased after nociceptor stimulation with capsaicin (fig. S10D). The addition of a CGRP receptor antagonist, olcegepant, to nociceptor-conditioned medium attenuated this effect (Fig. 6B). CGRP up-regulated pro–IL-1β in DCs within 1 hour, reaching a plateau within 4 hours (fig. S10E). Therefore, CGRP pretreatment enhanced the release of mature IL-1β from DCs upon inflammasome activation (fig. S10F). Finally, CGRP admixture to IMQ also significantly increased pro–IL-1β up-regulation in activated DCs. Simultaneously, CGRP at high concentrations exerted a moderate inhibitory effect on IL-12 p40 up-regulation (fig. S10G). This cytokine pattern implies that the DC response to CGRP is independent of and distinct from canonical DC activation mediated by PAMP receptor ligation.

To further explore the impact of nociceptor-derived CGRP, we compared the transcriptomes of DCs cocultured with nociceptors with those treated with CGRP or SP. Exposure to SP did not significantly alter the transcriptional profile of DCs (Fig. 6C and fig. S11A), in agreement with the present data and with published datasets (*10*, *42*), which indicates a lack of SP receptors on BMDCs (fig. S11B). Conversely, CGRP treatment resulted in profound transcriptional changes, reminiscent of, but not identical to, those observed in nociceptor cocultures

(Fig. 6C and fig. S11, A and C), suggesting that CGRP is a major, but not the only, nociceptor-derived signal modulating steady-state DCs. The accumulation of CGRP in the culture media of unstimulated neuronal cultures (fig. S10D) explains why the transcriptional profile of DC–nociceptor cocultures with or without capsaicin showed only minimal differences (fig. S8B). Because of the high sensitivity of DCs toward CGRP, the basal CGRP concentration in conditioned medium was apparently sufficient for a full-fledged DC response, rendering a further capsaicin-induced increase in CGRP functionally irrelevant.

CGRP enhances pro–IL-1β in DCs by signaling through a cAMP-p38–dependent pathway

The CGRP receptor comprises a G protein–coupled receptor (GPCR), which is the signal-transducing unit, and receptor-activity modifying protein 1 (RAMP1), which confers ligand specificity (*43*). Several G-protein subunits interact with this receptor, including $\alpha_{i/o}$, α_q, and α_s. Functionally, $G\alpha_{i/o}$ signaling reduces adenylyl cyclase (AC) activity, whereas $G\alpha_s$ signaling activates AC and promotes cyclic AMP (cAMP) accumulation, activating protein kinase A (PKA) (*43*) and certain mitogen-activated protein kinases (MAPKs) (*44*). To determine the pathways involved in CGRP-mediated pro–IL-1β up-regulation in DCs, we tested small-molecule inhibitors and activators of the respective enzymes. A PKA inhibitor, H89, showed no effect, whereas a p38 MAPK inhibitor, doramapimod, abrogated CGRP-induced pro–IL-1β expression. Conversely, an AC activator, forskolin, triggered pro–IL-1β expression in DCs, even in the absence of CGRP (Fig. 6D). Both CGRP and forskolin induced rapid phosphorylation of p38 (Fig. 6E), consistent with a model in which p38 activation lies downstream of CGRP-mediated AC activation. Additionally, 8-Br-cAMP, a hydrolysis-resistant synthetic analog of cAMP, drove pro–IL-1β accumulation in DCs (fig. S11D), and pertussis toxin–mediated inhibition of $G\alpha_{i/o}$ signaling further potentiated the effect of CGRP (fig. S11E).

Finally, surface-immobilized CCL2 enhanced the DC response to CGRP (Fig. 6E). CCR2 is a $G\alpha_i$-coupled GPCR, so CCR2 signaling might limit the availability of $G\alpha_i$ subunits, resulting in enhanced $G\alpha_s$ coupling to the CGRP receptor and increased cAMP signaling. Thus, in DCs, CGRP receptor signaling through $G\alpha_s$ promotes cAMP accumulation and initiates a p38-dependent program of gene expression (fig. S11F). Indeed, GSEA confirmed an enrichment of MAPK and p38 MAPK pathway genes in DCs after coculture with nociceptors (fig. S11G). This reprogramming is molecularly distinct from classical activation and renders DCs in a poised state of enhanced sentinel function characterized by intracellular accumulation of pro–IL-1β, as well as the up-regulation of genes important for pathogen resistance, regulation of phagocytosis, cell adhesion and migration, cytokine responsiveness, and antigen presentation (table S1).

Nociceptors promote cytokine production by dermal DCs in vivo

Having identified three distinct mechanisms by which nociceptors modulate DC functions in vitro, electrical activity, release of CGRP, and secretion of CCL2, we sought to determine their in vivo relevance by examining mice in which nociceptors had been ablated by treatment with resiniferatoxin (RTX). As shown previously (*9*) in mice with intact nociceptors, topical treatment with IMQ stimulated the production of IL-12 p40 and an influx of monocytes and neutrophils, a response that was markedly attenuated in RTX-treated animals (Fig. 7A and fig. S12A). Consistent with our in vitro observations, this correlated with a markedly lower frequency of IL-12 $p40^+$ dermal DCs in nociceptor-depleted mice (fig. S12B) even though the overall number of dermal DCs in steady-state skin was unaffected (fig. S12C). Similarly, blocking nociceptor electrical activity by topical treatment with lidocaine and QX-314 mimicked the effect of denervation and prevented IMQ-induced IL-12 p40 accumulation, as well as monocyte and neutrophil influx into the skin (Fig. 7B and fig. S12D). Finally, as predicted in vitro, both nociceptor depletion and anesthetics also decreased the accumulation of IL-6 (Fig. 7, C and D). Thus, the ablation of nociceptors and the pharmacological silencing of their electrical activity using topical anesthetics ameliorate the pathology that drives DC-dependent psoriasiform skin inflammation.

CGRP induces pro–IL-1β up-regulation in dermal DCs in vivo

In contrast to our in vitro experiments, in which the presence of nociceptors was sufficient to up-regulate pro–IL-1β in DCs (Fig. 6A), the in vivo ablation of nociceptors did not alter baseline levels of pro–IL-1β in dermal DCs (Fig. 7E). This was likely due to the fact that nociceptors in vitro spontaneously release CGRP (*45*), whereas resting nociceptors in vivo do not (*46*). Accordingly, when control mice were topically challenged with IMQ, dermal DCs responded by upregulating pro–IL-1β (Fig. 7E), resulting in the accumulation of mature IL-1β in the tissue (Fig. 7F). By contrast, IMQ had only a minimal effect on pro–IL-1β expression and IL-1β accumulation in animals in which nociceptors had been depleted (Fig. 7, E and F) or silenced (Fig. 7, G and H) in a manner analogous to the IL-12 p40 response. However, local treatment with capsaicin, a stimulus for nociceptors, but not DCs, failed to induce IL-12 p40 (fig. S12E), whereas pro–IL-1β was readily up-regulated in nociceptor-sufficient animals, an effect that was significantly dampened in RTX-treated mice (Fig. 7I). These findings were consistent with our in vitro observations that neuronal activation alone was insufficient to drive IL-12 p40 expression in otherwise unstimulated DCs (Fig. 1I). Capsaicin treatment also weakly induced pro–IL-1β up-regulation in RTX-treated animals (Fig. 7I), possibly because of incomplete nociceptor depletion or capsaicin-mediated activation of cutaneous mast cells, which may express TRPV1 (*47*), CGRP (fig. S12F), and other factors that could induce pro–IL-1β up-regulation in DCs (*48*).

To determine whether the induction of pro–IL-1β in DCs in vivo is CGRP dependent, we induced sterile tissue inflammation by intradermal corn oil injection. Admixture of olcegepant to the injectate decreased pro–IL-1β up-regulation in DCs, but had no impact on the influx of inflammatory cells (Fig. 7J and fig. S12G). Thus, the activation of nociceptors and resultant local release of CGRP are sufficient to drive pro–IL-1β up-regulation in dermal DCs independently of other inflammatory signals.

Nociceptor-derived CCL2 controls DC-dependent dermal immune responses

Finally, we assessed the role of nociceptor-derived CCL2. First, to determine CCL2 expression in nociceptors, we examined *Ccl2-mCherry*$^{fl/fl}$ reporter mice, which express a CCL2-mCherry fusion protein deletable by Cre recombinase (*49*). CCL2-mCherry was readily detectable by confocal microscopy within intra-axonal vesicle–like structures in cutaneous fibers at steady state (Fig. 8A) and after IMQ treatment (fig. S13A). CCL2 expression was not restricted to nociceptors, indicating that nociceptors are not the sole source of CCL2 in murine skin. Indeed, when *Ccl2-mCherry*$^{fl/fl}$ mice were crossed with *Scn10a*$^{Cre/+}$ mice (hereafter called NaV1.8$^{\Delta CCL2}$), the CCL2 reporter signal in non-neuronal cells remained unchanged but was extinguished in cutaneous nerve fibers (Fig. 8B and fig. S13B).

Upon topical treatment with IMQ, NaV1.8$^{\Delta CCL2}$ animals exhibited smaller inflammatory infiltrates (Fig. 8C) and decreased IL-12 p40 accumulation in the skin (Fig. 8D) compared with Cre-negative littermates. Dermal DCs expressed high levels of CCR2 (fig. S13C), indicating that they were equipped to sense and respond to CCL2. Nonetheless, the number of DCs in unperturbed skin was comparable between NaV1.8$^{\Delta CCL2}$ animals and littermate controls (fig. S13D), suggesting that nociceptor-derived CCL2 was dispensable for the maintenance of dermal DCs under steady-state conditions. After IMQ treatment, however, NaV1.8$^{\Delta CCL2}$ mice showed a decrease in dermal DC numbers compared with their littermates (Fig. 8E), suggesting that nociceptor-derived CCL2 serves as a retention signal preventing DCs from prematurely leaving the skin, thus allowing for a

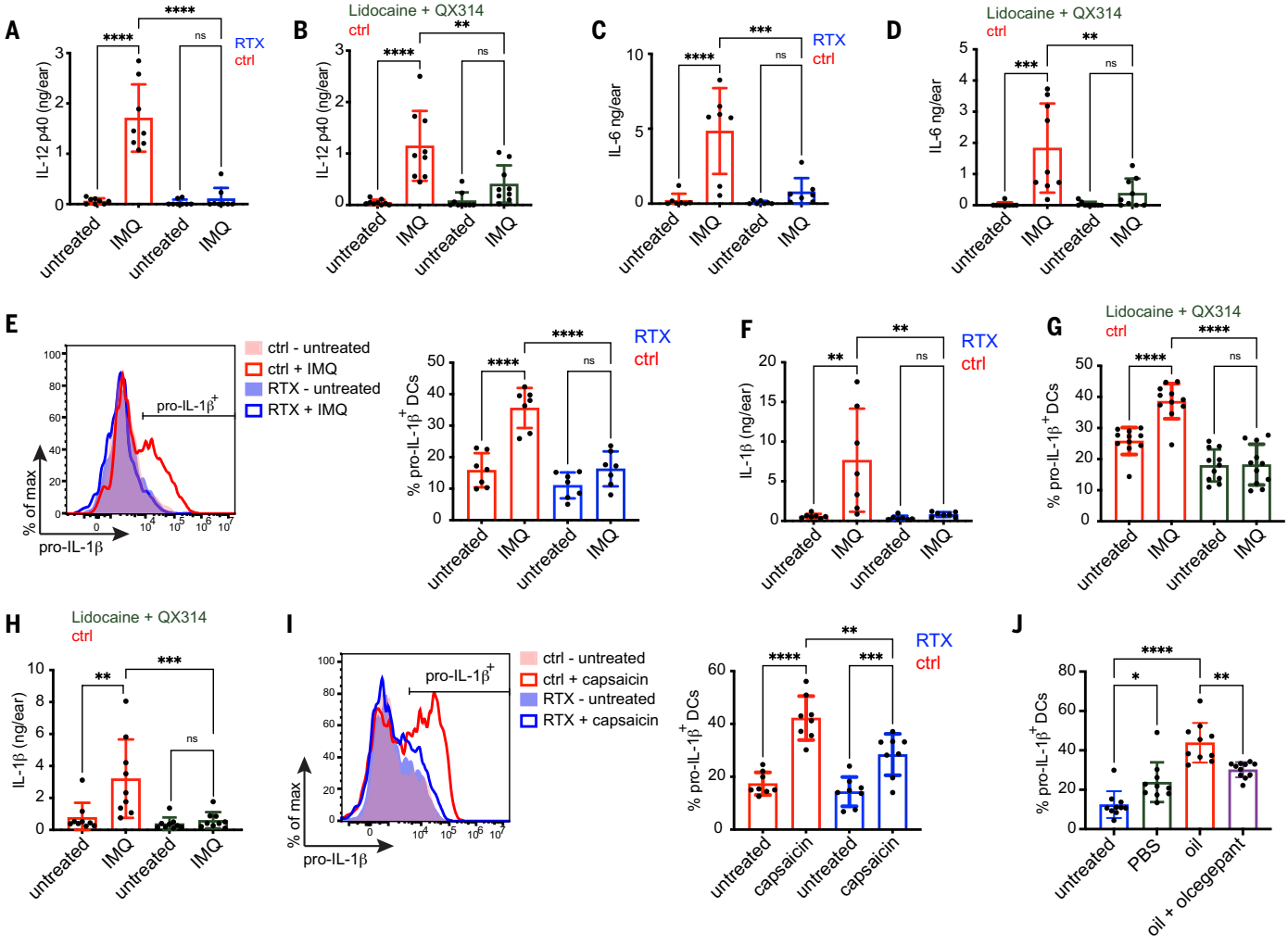

Fig. 7. Nociceptors control DC functions in murine skin in vivo. (**A** to **D**) Ears of mice in which nociceptors had been left intact, were chemically ablated, or were treated with lidocaine + QX314 were then treated topically with IMQ cream. Cytokine accumulation was analyzed by tissue lysate ELISA. Summary of three to four experiments (n = 7-9 per group) is shown. (**E**) Ears of mice in which nociceptors had been left intact or were chemically ablated were treated with IMQ cream, and pro–IL-1β expression by dermal DCs was assessed by flow cytometry. One representative experiment (left) and quantification of three independent experiments (n = 7 per group; right) are shown. (**F**) Ears of mice were treated as in (E) and the accumulation of mature IL-1β cytokine in the tissues was assessed by by tissue lysate ELISA. Summary of three experiments (n = 7 per group) is shown. (**G**) Ears of mice in which nociceptors had been left intact or ears treated with lidocaine + QX314 were treated topically with IMQ cream, and pro–IL-1β expression by dermal DCs was assessed by flow cytometry. Summary of five experiments (n = 11 per group) is shown. (**H**) Ears of mice were treated as in (G) and the accumulation of mature IL-1β cytokine in the tissues was assessed by by tissue lysate ELISA. Summary of three experiments (n = 9 per group) is shown. (**I**) Ears of mice in which nociceptors had been left intact or were chemically ablated were treated with capsaicin and analyzed for pro–IL-1β expression by flow cytometry. One representative experiment (left) and quantification of four independent experiments (n = 8 per group; right) are shown. (**J**) Mouse ears were injected intradermally with PBS, oil, or oil supplemented with olcegepant, and pro–IL-1β up-regulation in DCs was analyzed by flow cytometry 16 hours later. Quantitation of four independent experiments (n = 10 to 11 per group) is shown. Across all panels, data represent mean ± SD. Two-way ANOVA with Tukey's multiple-comparisons test was used for statistical analysis: $^{*}P < 0.05$, $^{**}P < 0.01$, $^{***}P < 0.001$, $^{****}P < 0.0001$.

longer period of in situ cytokine production and more pronounced local inflammation.

In addition to compromising local inflammatory responses, we reasoned that the dysregulation of DC migration may also interfere with the acquisition of cutaneous antigens and affect the initiation of adaptive immune responses. To test this idea, we performed contact hypersensitivity (CHS) experiments in which the adaptive recall response depends on the acquisition of hapten-modified self-antigens by dermal DCs and their presentation to adaptive lymphocytes in draining lymph nodes (*50*). In naïve mice, exposure of ear skin to hapten caused a comparable irritant response in NaV1.8$^{\Delta CCL2}$ animals and littermates. By contrast, the DC-dependent recall response in mice sensitized by prior hapten painting of abdominal skin was nearly abrogated in the absence of nociceptor-derived CCL2 (Fig. 8F and fig. S13E). Nociceptor ablation has previously been shown to impair the ability of DCs to acquire viral antigens in HSV-1–infected skin (*51*), suggesting that this phenotype of NaV1.8$^{\Delta CCL2}$ mice was likely caused by a defect in DC-dependent priming of antigen-specific lymphocytes in lymph nodes. Indeed, when WT mice were treated with lidocaine and QX-314 to transiently inhibit nociceptor activity in abdominal skin during sensitization, the CHS response was compromised

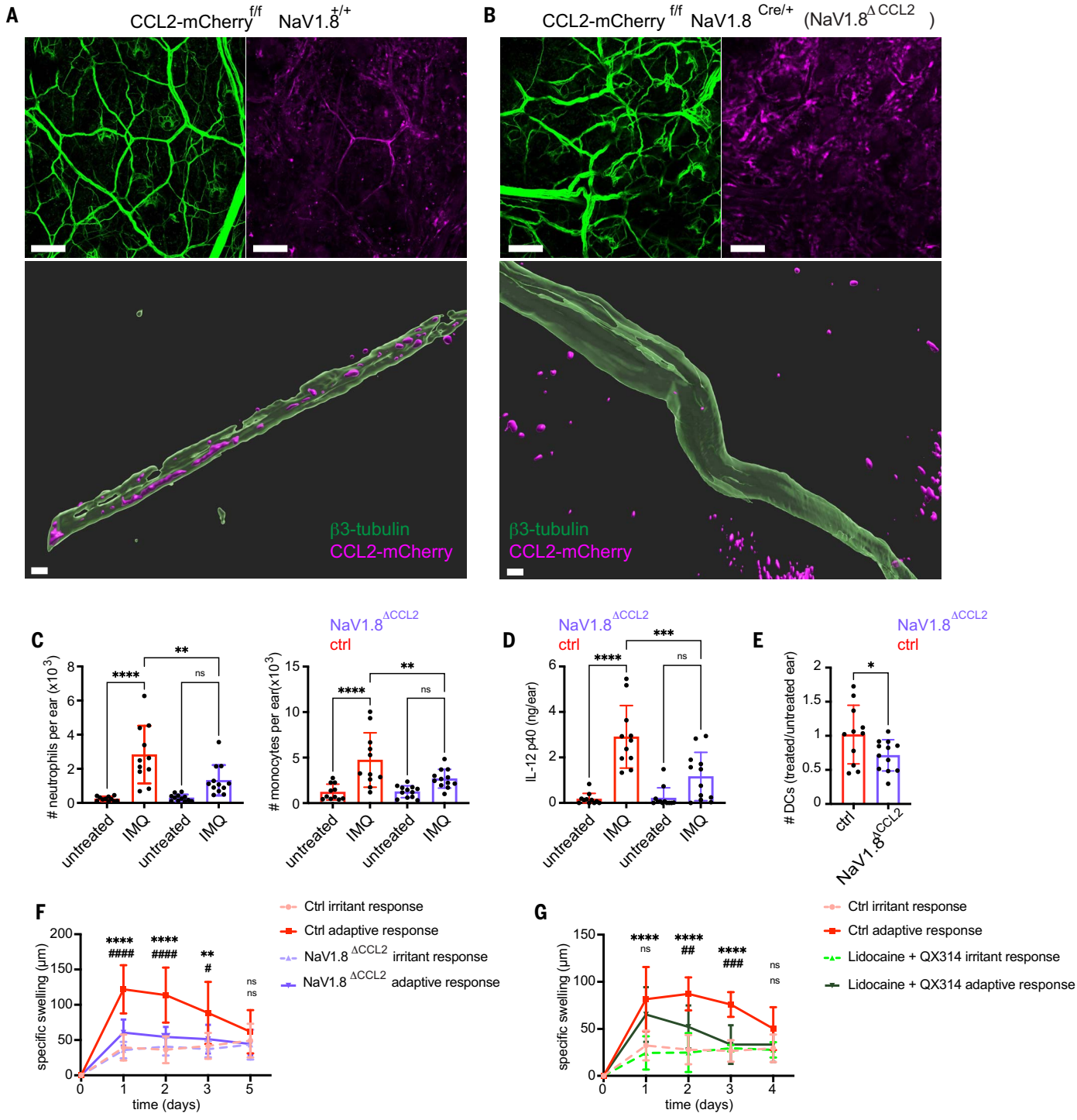

Fig. 8. Nociceptor-derived CCL2 is important for induction of local inflammatory and adaptive immune responses. (**A** and **B**) Dermal sheets from NaV1.8$^{+/+}$ CCL2-mCherry (control) (A) and NaV1.8$^{Cre/+}$ CCL2-mCherry (NaV1.8$^{\Delta CCL2}$) (B) animals were fixed, stained with anti–β3-tubulin (green) and anti-mCherry (magenta) antibodies, and analyzed using confocal microscopy. Examples of neuronal fibers showing CCL2-mCherry signal are highlighted with arrows (top panels). Surface reconstructions of high-resolution images were performed in Imaris to illustrate the vesicle-like staining pattern of CCL2 (bottom panels). Scale bars: 100 μm in top panels and 2 μm in bottom panels. (**C** to **E**) Ears of NaV1.8$^{\Delta CCL2}$ or littermate control mice were treated with IMQ cream and inflammatory infiltrate (C) and IL12-p40 accumulation (D) and ratios of DCs between treated and untreated ears for each animal (E) were analyzed. Summary data of six experiments (n = 11 to 12 per group) is shown. (**F** and **G**) Mice were sensitized with DNFB or treated with vehicle control (acetone) and challenged 5 days later with DNFB on one ear and acetone on the other. Ear thickness was measured at the indicated time points after challenge, and specific swelling was calculated as the difference between the DNFB-treated ear and the vehicle-treated ear for each animal. (F) NaV1.8$^{\Delta CCL2}$ or littermate control mice (n = 7 to 8 per group). (G) WT mice treated with lidocaine + QX314 before

and on 2 consecutive days after sensitization. All data are presented as mean ± SD. Two-way ANOVA with Tukey's multiple-comparisons test was used for statistical analysis. For (F) and (G), *statistical comparison between control DNFB-sensitized and control nonsensitized groups and #statistical comparison between control DNFB-sensitized and NaV1.8$^{\Delta CCL2}$ DNFB-sensitized groups (F) or between control DNFB-sensitized and lidocaine + QX314 DNFB-sensitized groups (G). *, #P < 0.05; **, ##P < 0.01; ***, ###P < 0.001; ****, ####P < 0.001.

in subsequently challenged ear skin where nociceptors had always been fully functional (Fig. 8G and fig. S13F). Thus, nociceptors must be functional and express CCL2 for the proper induction of both DC-dependent local inflammation and the priming of adaptive immune responses against dermal antigens.

Discussion

At the transcriptome level, our results indicate that the presence of nociceptors induces numerous subset-specific changes in cDC1 and cDC2 cells in vitro. These differential responses likely reflect the fact that cDC1s and cDC2s have distinct roles in regulating immune responses, and it will be important to determine whether and how nociceptors regulate subset-specific cDC functions in vivo. The present study has, however, focused on exploring the communication signals emanating from nociceptors that elicit a shared response by all cDCs in peripheral tissues.

We show here that nociceptors control DC functions in a context-dependent manner through at least three independent communication modalities. Without immune stimuli, nociceptor-derived CGRP induces transcriptional changes in steady-state DCs to up-regulate sentinel function–related genes but without causing overt DC activation. Upon concomitant encounter of painful stimuli and PAMPs, the nociceptors' electrical activity is sensed by interacting PAMP-stimulated DCs, which increases the proportion of DCs that commence the production of proinflammatory cytokines. Thus, DCs are uniquely equipped to sense and interpret nociceptor activation either as a "reminder" to assume a poised, anticipatory state when other inflammatory signals are absent or as an "alarm call" that amplifies their collective inflammatory response to immune stimuli. Additionally, by secreting CCL2, nociceptors further fine-tune DC functions by promoting their contribution to local inflammatory responses and by regulating the egress of DCs from the skin to optimize adaptive immune responses (fig. S14).

CGRP receptor–mediated activation of AC (*52*) exerts anti-inflammatory effects on immune cells, including macrophages (*53*), neutrophils (*46*), γδT cells (*54*), and innate lymphoid cells (*55*). By contrast, CGRP, even at high concentrations, had only modest inhibitory effects on IL-12 p40 up-regulation in activated BMDCs (figs. S4E and S10G). This was in contrast to previously reported inhibitory effects of CGRP on IL-12 production in granulocyte-macrophage colony-stimulating factor (GM-CSF)–induced BMDCs (*11*). Unlike the Flt3L-induced BMDCs used here, GM-CSF cultures contain macrophages (*56*), which are potently inhibited by nociceptors (Fig. 1D) and by CGRP (*52*). It is therefore possible that the negative effect of CGRP on GM-CSF–induced BMDC cultures may be a consequence of macrophage contamination rather than a true effect on DCs. Finally, taken at face value, these observations also suggest an inherent difference in the intracellular signaling pathways between DCs and macrophages whereby AC activation may exert strong inhibitory effects on the latter (*57*) but not the former.

In light of the exquisite sensitivity of DCs toward CGRP, the close proximity of DCs and nociceptors in vivo, and the anticipatory nature of the DC response elicited by CGRP, it is tempting to speculate that DCs may have specifically evolved to register and interpret a local, limited release of CGRP induced by transient or subtle activation of nociceptors as a warning signal that could portend a barrier breach. By contrast, other immune cells that do not a priori associate closely with nociceptors may only sense CGRP when it is released in larger quantities, likely as a consequence of severe tissue damage. In this context, CGRP-induced anti-inflammatory and tissue repair–promoting functions [e.g., through action on macrophages (*57*) or neutrophils (*46*)] may become more prominent.

Although CGRP did not induce IL-23 production by DCs in this study, recent work has demonstrated that nociceptor-derived CGRP is sufficient and necessary for IL-23 production by CD301b$^+$ dermal DCs during *C. albicans* infection (*8*). The reasons for this discrepancy remain unclear, but it is possible that CGRP-induced IL-1β potentiates IL-23 expression (*58*, *59*) or that an intermediary cell type(s) that generates as-yet-unidentified secondary signals in response to CGRP to promote IL-23 production by DCs may be involved.

Aside from neuropeptides, our results highlight a critical role for CCL2, a chemokine whose expression by nociceptors has traditionally been considered a sign of pathology. CCL2 can recruit inflammatory cells to DRGs, resulting in peripheral sensitization and neuropathic pain (*60*). However, some nociceptors express CCL2 even at steady state, at least at the mRNA level (*3*, *61*, *62*). Indeed, we show here that the expression of CCL2 in cutaneous fibers is not necessarily maladaptive but rather serves to fine-tune DC-dependent immune responses. Aside from DCs, other cell types, including monocytes and memory T-cell subsets, also express the CCL2 receptor CCR2; however, the impact of nociceptor-derived CCL2 on these populations remains to be explored. Moreover, further work will be needed to determine how CCL2 is regulated in nociceptors. In vitro, cultured nociceptors released CCL2 spontaneously, and nociceptor stimulation further potentiated CCL2 release, similar to the dynamics of neuropeptide release. In vivo, neuropeptide release from nociceptors is tightly controlled (*46*), but it remains to be established whether similar rules apply to CCL2.

Although myeloid leukocytes are generally not considered excitable, we observed that activation of nociceptors induced membrane depolarization and calcium flux in the interacting DCs. Spreading of action potentials to and among non-neural cells through mechanisms including gap junctions and tunneling nanotubes has been described previously (*63*), and both of these communication modalities have been reported for DCs (*64*). Whatever the mechanism, our observations establish a precedent for a direct, contact-dependent, and neuropeptide-independent communication pathway between nociceptors and DCs, which culminates in calcium mobilization in the latter. Intracellular calcium is a key second messenger in numerous signaling processes. The downstream molecular signaling pathway(s) promoting DC production of IL-12 p40 and IL-6 but not TNFα remains to be clarified. Nonetheless, synergy between MyD88- and TRIF-dependent pathways in DCs has previously been shown to stimulate IL-12 and IL-6 secretion while having no effect on TNFα (*65*), indicating that these cytokines are not co-regulated. Conceivably, calcium mobilization in activated DCs triggered by firing nociceptors might act in an analogous manner to synergize with TLR-induced MyD88 signaling to potentiate the expression of IL-12 p40 and IL-6.

Materials and Methods

Mice

C57BL/6J (JAX stock no. 000664), *Ccl2*$^{-/-}$ (JAX stock no. 004434) (*26*), *Tlr7*$^{-/-}$ (JAX stock no. 008380) (*17*), *Zbtb46*^{eGFP} (JAX stock no. 027618) (*30*), and *Ccl2-mCherry*$^{fl/fl}$ (JAX stock no. 016849) (69) mice were purchased from The Jackson Laboratory. *I-A*^{b}β-eGFP (*66*), *Scn10a*^{Cre} (*67*), and *Scn10a*$^{Cre/Cre}$*Rosa26*$^{TdT/TdT}$ (*3*) mice were all described previously and were bred at the Harvard Medical School animal facility. All animal experiments were performed in accordance with national and institutional

guidelines, and were approved by the institutional animal care and use committee and the Committee on Microbiological Safety (COMS) of Harvard Medical School. Both male and female mice were used.

In vitro DC generation

Flt3L-induced BM-derived dendritic cells were generated as described previously (*68*). Briefly, BM was harvested from femurs and tibiae of 6- to 8-week-old C57BL/6J mice of either sex. Red blood cells were lysed and BM cells were plated with 100 ng/ml recombinant Flt3L (R&D Systems) in six-well plates (3 ml per well), one plate per mouse in RPMI1640 medium (Gibco) containing 10% fetal bovine serum (FBS) (Gemini Bio), β-mercaptoethanol, glutamine, and penicillin–streptomycin. Fully developed DCs were harvested and used on days 9 and 10.

In vitro macrophage generation

M-CSF–induced BM macrophages were generated as described previously (*69*). Briefly, BM was harvested from femurs and tibiae of 6- to 8-week-old C57BL/6J mice of either sex. Red blood cells were lysed and BM cells were plated with 25 ng/ml recombinant M-CSF in six-well plates (3 ml per well) in RPMI1640 medium (Gibco) containing 10% FBS (Gemini Bio), β-mercaptoethanol, glutamine, and penicillin–streptomycin. Fully developed macrophages were harvested and used on day 7.

In vitro nociceptor culture

DRG cultures were prepared from freshly isolated dorsal root ganglia from adult (6- to 10-week-old) C57BL/6J mice of either sex as described previously (*45*, *70*) with minor modifications. Briefly, the dissection was performed in ice-cold phosphate-buffered saline (PBS), and harvested DRGs were kept on ice throughout. The first step of digestion was performed for 10 min at 37°C in 3 ml of Hank's balanced salt solution (HBSS) (Gibco) with 60 U of papain (Worthington), 0.5 mM EDTA, and 1.5 mM $CaCl_2$. The second digestion step was performed in 3 ml of HBSS with 4 mg/ml collagenase Type-2 (Worthington) and 5 mg/ml dispase (Gibco) for 30 min at 37°C. Cell suspensions were triturated by repeated pipetting in Leibovitz medium (Gibco) supplemented with 10% FBS (Gemini Bio), overlaid over 20% Percoll (GE Healthcare) in Leibovitz medium, and centrifuged for 9 min at 400*g* with no brake. Pelleted cells were washed in Neurobasal Medium (Gibco) containing B27 supplement (Gibco) and penicillin–streptomycin before being plated ($1\text{-}1.5\times10^4$ cells per well) in wells precoated with poly-D lysine and laminin (both Sigma Aldrich) in Neurobasal Medium containing B27 supplement and penicillin–streptomycin, supplemented with 5 μM cytosine β-D-arabinofuranoside (Sigma-Aldrich) and 25 ng/ml mouse recombinant NGF (R&D Systems). Culture medium was refreshed every 4 to 5 days, and neuronal culture was typically used between days 7 and 10 after plating. Cultures were visually inspected to verify neuronal recovery and depletion of contaminating glial/Schwann cells before each experiment.

In vitro cortical and hippocampal neuron cultures

CNS neuronal cultures were prepared from freshly isolated C57BL/6J mouse embryonic day 18 (E18) to E19 brains, as described previously (*71*) with minor adjustments. Dissection was performed in ice-cold HBSS + HEPES (both Gibco), and tissues were digested at 37°C for 15 min in 0.25% trypsin (Invitrogen) for hippocampus and 0.25% trypsin + 0.5 mg/ml DNAse I (Roche) for cortex samples. Tissues were homogenized by trituration in a fire-polished Pasteur pipette, and single-cell suspensions were generated by filtration through 100-μm cell strainers. Cells were washed in Neurobasal Medium containing B27 supplement (both Gibco) and penicillin–streptomycin before being plated in wells precoated with poly-D-lysine and laminin (both Sigma-Aldrich) in Neurobasal Medium containing B27 supplement and penicillin–streptomycin supplemented with 5 μM cytosine β-D-arabinofuranoside (Sigma-Aldrich). Culture medium was refreshed every 3 days, and the culture was used between days 7 and 14 after plating.

In vitro cocultures

For coculture experiments, neuronal medium was replaced with fresh Neurobasal Medium containing B27 supplement and penicillin–streptomycin, and 1×10^5 BMDCs per well were added in an equal volume of RPMI 1640 medium containing 10% FBS, β-mercaptoethanol, glutamine, and penicillin–streptomycin. Cells were allowed to interact for 2 to 4 hours before any treatments or stimuli were applied unless stated otherwise. As a control, DCs were plated and treated in an identical fashion in wells containing an appropriate volume of Neurobasal Medium with B27 supplement and penicillin–streptomycin but no nociceptors.

In vitro treatments

All treatments were performed overnight unless otherwise stated. All CGRP treatments were performed with 1 nM CGRP unless otherwise indicated. Lidocaine (500 μM), QX314 (1 mM), A967079 (10 μM), and olcegepant (100 nM) were added to cultured nociceptors 2 hours before the addition of DCs. H89 (1 μM), doramapimod (1 μM), and pertussis toxin (100 ng/ml) were added to DCs immediately before CGRP treatment. 8-Br-cAMP (1 mM) and forskolin (50 μM) were used without further stimuli. A23187 (400 ng/ml) was added to DCs alongside IMQ, and the treatment lasted for 4 to 5 hours to avoid toxicity. Activating stimuli were used at the following concentrations: IMQ, 1 μg/ml; zymosan, 10 μg/ml; LPS, 1 ng/ml; flagellin, 20 ng/ml; CpG, 0.1 μM; poly I:C, 1 μg/ml; PR-8 GFP IAV, multiplicity of infection (MOI) = 0.25; *S. pneumoniae*, MOI = 5; and *C. albicans*, MOI = 10.

Microbes

Influenza PR8-GFP was generously provided by Dr. A. Garcia-Sastre at the Mount Sinai School of Medicine and the NIAID Centers of Excellence for Influenza Research and Surveillance program. *S. pneumoniae* was a kind gift from Dr. R. Malley at the Boston Children's Hospital and Harvard Medical School. *C. albicans* was purchased from ATCC (MYA-2876).

ELISA

ELISA kits specific for IL-12 p40 (catalog no. 431601), IL-6 (catalog no. 431302), TNFα (catalog no. 430902), IFN-β (catalog no. 439407), CCL2 (catalog no. 432704), and IL-1β (catalog no. 432603) were from BioLegend. The EIA kit specific for CGRP (catalog no. 589001) was from Cayman Chemicals. All assays were performed as per the manufacturers' instructions.

In vitro coculture flow cytometry analysis

In vitro cultures were harvested in warm 5 mM EDTA in PBS. Dead cells were then stained using the LIVE/DEAD Fixable Near-IR Dead Cell Stain Kit (Thermo Fisher) in ice-cold PBS. Samples were washed and stained with fluorescent antibodies for appropriate surface markers in fluorescence-activated cell sorting (FACS) buffer (1% FBS, 5 mM EDTA, and 0.1% NaN_3 in PBS) on ice. Intracellular staining was performed using the Cytofix/Cytoperm kit (BD Biosciences) according to the manufacturer's instructions. cDC1s were identified as $XCR\text{-}1^+$, and cDC2s were identified as $CD11b^+$. For IL-6 intracellular stains, 10 μM brefeldin A was added to the cultures 2 hours before harvest.

Transwell assays

BMDCs (0.5 to 1×10^6) in complete RPMI 1640 medium were added to the upper compartment of a Transwell setup (Corning) with 5-μm pores and allowed to migrate into the lower compartment containing chemotactic stimuli for 4 hours. Migrated cells were harvested, stained with fluorescent antibodies, and enumerated by flow cytometry. The chemotactic index was calculated as the number of cells transmigrated under a given condition divided by the number of cells that transmigrated between two compartments containing the same medium.

Chemotactic molecule identification

The Mouse Chemokine Array C1 (Ray Biotech) and Proteome Profiler Mouse Chemokine Array Kit (R&D) were used. Membranes were incubated with nociceptor-conditioned medium or control medium overnight and developed

as per the manufacturers' instructions. The signal intensity for each spot was quantified in Fiji 2.0.0 (72) using the Analyze Gels function.

SDS-PAGE and immunoblot analysis

Cells were harvested and lysed for 30 min in Tris buffer, pH 7.5, with 1% SDS, 150 mM NaCl, 10 mM NaF, 2 mM Na_3VO_4, protease inhibitors (Thermo Scientific), and benzonase (Sigma Aldrich). After 30 min, the lysate was diluted 1 to 10 into Tris buffer, pH 7.5, with 1% NP40, 150 mM NaCl, 10 mM NaF, 2 mM Na_3VO_4, and protease inhibitors (Thermo Scientific) and centrifuged for 15 min at 16,000*g*. Supernatants were prepared for SDS–polyacrylamide gel electrophoresis (SDS-PAGE) in 6× Laemmli buffer containing 60% v/v glycerol, 150 mg/ml SDS, and 0.75 mg/ml bromophenol blue in 75 mM Tris–HCl, pH 6.8, in the presence of 100 mM dithiothreitol. Separation was performed using 4 to 12% NuPAGE precast gels (Invitrogen). Proteins were transferred onto Immobilon P membrane (Merck Millipore) using wet transfer, and the membrane was blocked in 5% bovine serum albumin (BSA) in PBS + 0.05% Tween-20. Binding of appropriate horseradish peroxidase–conjugated antibodies was revealed using Luminata Forte HRP substrate (Merck Millipore) and Amersham Imager 600 (GE Healthcare).

Live-cell imaging

Live-cell imaging was performed on a Nikon Ti inverted microscope equipped with W1 Yokogawa Spinning disk with 50-μm pinholes, an Andor Zyla 4.2 Plus sCMOS monochrome camera, and the OKO Lab Heated enclosure with environmental control set to 37°C and 5% CO_2. A Plan Apo λ 20X/0.75 DIC I objective was used. All imaging experiments were performed in a 1:1 mixture of RPMI 1640 medium containing 10% FBS, β-mercaptoethanol, glutamine, and penicillin–streptomycin and Neurobasal Medium containing B27 supplement and penicillin–streptomycin, both phenol red–free, on μ-Slide eight-well chambered coverslips (Ibidi). For the microfluidics experiments, Xona Microfluidics chips with 150-μm microgrooves were used.

For calcium-imaging experiments, cells were loaded with 10 μM Fluo-4 calcium-sensitive dye (Thermo-Fisher) for 20 min at 37°C. Immediately before imaging, Fluo-4–containing medium was replaced with fresh, prewarmed, phenol red–free medium, and the Fluo-4 signal was imaged in a single confocal plane using a 488-nm laser line and a GFP filter cube (Chroma ET 49002).

For membrane potential imaging experiments using BeRST dye, cells were loaded with 5 μM BeRST and 10 μM Fluo-4 for 20 min at 37°C. Immediately before imaging, dye-containing medium was replaced with fresh, prewarmed phenol red–free medium, and images were acquired in a single confocal plane using 488- and 640-nm laser lines and GFP and Cy5 filter cubes (ET Chroma 49002 and 49006).

For membrane potential imaging experiments using Di-8-ANNEPS, cells were loaded with 5 μM Di-8-ANNEPS for 30 min at 37°C. Immediately before imaging, dye-containing medium was replaced with fresh, prewarmed medium, and images were acquired in a single confocal plane using a 488-nm laser line and mCherry and Cy5 filter cubes (ET Chroma 49008 and 49006).

Light-sheet imaging

The lattice light-sheet microscope was constructed as described previously (73) with a Special Optics 0.65 numerical aperture (NA) excitation objective, a Nikon CFI Apo LWD 25XW 1.1 NA detection objective, an Orca Flash 4.0 v3 sCMOS camera (Hamamatsu), and 488-nm (300 mW Coherent Sapphire) and 560-nm (500 mW, MPB Communications) lasers. The annular mask was set at 0.42 to 0.5 NA, and a square lattice in the dithered mode was produced at the sample. The excitation power (488 nm) was measured at the back focal plane of the excitation objective at ~100 μW. The 25× detection objective was paired with a 500-mm achromat lens for an effective magnification of 63.7×, resulting an image pixel size of 102 nm. The exposure time for each plane was 4 ms, and the stage-scanning step size for the volumetric imaging was 0.5 mm, corresponding to 265 nm along the optical axis after deskewing. Data were deskewed and deconvolved with LLSpy (DOI: 10.5281/zenodo.1059099) and cudaDeconv (source code available at https://github.com/scopetools/cudaDecon) using a PSF measured from a 0.1 μm bead. sCMOS residual charge artifact was corrected using LLSpy (https://llspy.readthedocs.io/en/latest/camera.html).

Electron microscopy

Nociceptors were grown on aclar coverslips precoated with poly-D-lysine and laminin. DCs were allowed to interact with nociceptors for 4 hours before the co-culture was fixed in a mixture of 2.5% glutaraldehyde, 1.25% paraformaldehyde, and 0.03% picric acid in 0.1 M sodium cacodylate buffer, pH 7.4, for 1 hour at room temperature. The cells were washed in 0.1 M sodium cacodylate buffer, pH 7.4, post-fixed for 30 min in a 1% OsO_4/1.5% $KFeCN_6$ solution, washed twice in water and once in maleate buffer, and incubated in 1% uranyl acetate in maleate buffer for 30 min. This was followed by two washes in water and subsequent dehydration in grades of alcohol (5 min each at 50, 70, and 95% and twice at 100%). The samples were subsequently embedded in TAAB Epon (Marivac Canada Inc.) and polymerized at 60°C for 48 hours. After polymerization, the aclar was peeled off, and ultrathin sections (~80 nm) were cut on a Reichert Ultracut-S microtome, picked up onto copper grids, and stained with lead citrate. Grids were examined under a TecnaiG^2 Spirit BioTWIN transmission electron microscope, and images were recorded using an AMT 2k CCD camera.

Confocal imaging

For whole-mount imaging of dermal sheets, ears of from Zbtb46^{eGFP}Scn10a$^{Cre/+}$ROSA$^{tdTomato/+}$ animals were split into the dorsal and ventral aspects, fixed in 4% paraformaldehyde (PFA), permeabilized in 0.3% Tween in PBS, and stained with S100β primary antibody overnight in a blocking buffer containing 3% BSA. Samples were washed and stained with anti-rabbit Alexa Fluor 647 and anti-GFP Alexa Fluor 488 antibodies. Ears of *Ccl2-mCherry*$^{fl/fl}$ or Scn10a$^{Cre/+}$*Ccl2-mCherry*$^{fl/fl}$ animals were split into the dorsal and ventral aspects, fixed in 4% PFA, permeabilized in 0.3% Tween in PBS, blocked in 3% BSA, and stained with β3-tubulin and mCherry antibodies for 48 hours. Subsequently, the samples were washed and stained with anti-goat Alexa Fluor 568 and anti-rabbit Alexa Fluor 647 antibodies.

For imaging of fixed nociceptor cultures, nociceptors isolated from NaV1.8$^{Cre/+}$Rosa26$^{tdTomato/+}$ were plated on μ-Slide eight-well chambered coverslips (Ibidi), and cultures were maintained as per the standard protocol. Cells were fixed in 4% PFA, permeabilized in 0.3% Tween in PBS, and stained with β3-tubulin primary antibody overnight in a blocking buffer containing 3% BSA. Samples were then washed and stained with anti-rabbit Alexa Fluor 488 antibody.

Images were acquired on an Olympus IX83 inverted single-point laser scanning confocal microscope with UPlan S Apo 20×/0.75 air or UPlan X Apo 60×/1.42 oil objectives.

Image analysis

Calcium imaging and membrane potential analysis were performed in Fiji 2.0.0 (72). Images are presented using the "Fire" LUT, and quantitation of signal was performed in selected regions of interest across all time points using the "Plot Z-axis profile" function to generate single-cell response graphs. For statistical analysis, cells were manually traced and were considered "responders" if their Fluo-4 signal showed at least 50% increase ($F_{max}/F_0 \geq 1.5$), "equivocal" for a 30 to 50% increase ($1.5 > F_{max}/F_0 \geq 1.3$), and "nonresponders" if no change >30% was observed ($F_{max}/F_0 < 1.3$). Only cells observed contacting a firing axon were considered in the coculture condition.

For the ratiometric analysis of Di-8-ANNEPS imaging, both channels were background subtracted, and the ratio of channels was generated for each pixel. The resulting image was thresholded and is presented using the "Fire" LUT. A binary mask created from original images that included all neuronal bodies, as well as axons and DCs, was used to assign a zero value to background pixels.

3D reconstruction of confocal images of skin whole mounts and the generation of surfaces were performed in Imaris 9.2.1.

RNA-seq

CD45.1 BMDCs were incubated with nociceptors from CD45.2 mice or alone and treated with the appropriate stimuli. After 8 hours, the cultured cells were harvested, stained, and sorted on a MoFlo Astrios EQ FACS-sorter (Beckman). cDC1s were identified as CD45.1$^+$XCR-1$^+$CD11b$^-$, cDC2s as CD45.1$^+$CD11b$^+$XCR-1$^-$, and pDCs as CD45.1$^+$XCR-1$^-$CD11b$^-$PDCA1$^+$. One thousand cells of each population were sorted directly into 5 μl of lysis buffer (TCL Buffer from Qiagen with 1% β-mercaptoethanol), and Smart-seq2 libraries were prepared as previously described (*74*, *75*) with slight modifications. Briefly, total RNA was captured and purified on RNAClean XP beads (Beckman Coulter). Polyadenylated mRNA was then selected using an anchored oligo(dT) primer (5′-AAGCAGTGGTATCAACGCAGAGTACT30VN-3′) and converted to cDNA through reverse transcription. First-strand cDNA was subjected to limited polymerase chain reaction (PCR) amplification, followed by transposon-based fragmentation using the Nextera XT DNA Library Preparation Kit (Illumina). Samples were PCR amplified for 18 cycles using barcoded primers such that each sample carried a specific combination of eight base Illumina P5 and P7 barcodes, and samples were pooled together before sequencing. Paired-end sequencing was performed on an Illumina NextSeq500 using 2 × 25 bp reads.

RNA-seq data analysis

Reads were aligned to the mouse genome (GENCODE GRCm38/mm10 primary assembly and gene annotations vM16; https://www.gencodegenes.org/mouse/release_M16.html) with STAR 2.5.4a (https://github.com/alexdobin/STAR/releases). The ribosomal RNA gene annotations were removed from the GTF (general transfer format) file. The gene-level quantification was calculated by featureCounts (https://subread.sourceforge.net/). Raw reads count tables were normalized in iDEP.91 {EdgeR [Log2(CPM+1)]} (*76*). Samples with fewer than 2×10^6 uniquely mapped reads were excluded to mitigate the effect of poor-quality samples on normalized counts, and only genes with minimal 50 counts per million (CPM) expression in at least two libraries were selected for further analysis to exclude genes with little to no expression across all conditions. Differentially expressed genes were identified using DESeq2 with FC ≥ 2 and FDR 0.1 cutoffs in iDEP.91.

PCA was performed and visualized using Population PCA software (https://cbdm.hms.harvard.edu/LabMembersPges/SD.html) for 3D PCA, or prcomp function within the R3.6.1 package and visualized using ggbiplot for 2D PCA. Morpheus (https://software.broadinstitute.org/morpheus/) was used for visualization and heatmap generation. GSEA analysis (*37*, *38*) was performed in GSEA 4.0.1 software using the Hallmarks gene matrix v7.1 (h.all.v7.1) (*39*) and the Biocarta gene matrix v7.4 (c2.cp.biocarta.v7.4) MAPK_PATHWAY and P38_MAPK_PATHWAY subsets.

Antibodies

All antibodies used in this study are listed in table S2.

In vivo nociceptor depletion

RTX-mediated depletion of nociceptor innervation was performed as described previously (*9*). Four-week-old mice were injected on 3 consecutive days with 30, 70, and 100 mg/kg body weight of RTX or vehicle control and allowed to age for at least 6 weeks before being used for experiments. Functional denervation was confirmed using the tail withdrawal assay (*9*).

Imiquimod and capsaicin treatment in vivo

Eight- to 20-week-old C57BL/6J mice were treated topically with capsaicin or IMQ as described previously (*9*, *77*). Briefly, for capsaicin treatment, mice were anesthetized, and 250 μg of capsaicin [50 mM in dimethyl sulfoxide (DMSO)] was applied to the treated ear (125 μg on each side) twice 12 hours apart. Pro–IL-1β expression was assessed 24 hours after the first dose. For IMQ treatment, mice were anesthetized, and 25 mg of IMQ in the form of a 5% cream (Aldara) was applied to the treated ear three times 24 hours apart. Where indicated, 3 hours before the IMQ treatment, 5 mg of QX-314 and 5 mg of lidocaine in the form of 4% cream (Aspercreme) was applied to the treated skin. IL-1β, pro–IL-1β, IL-6, or IL-12 p40 expression was assessed 72 hours after the first treatment.

Intradermal injections

Six- to 10-week-old C57BL/6J mice were anesthetized, and 10 μl of PBS, corn oil with 10% DMSO, or corn oil with 10% DMSO and 5 mg/ml olcegepant was injected intradermally into the dorsal side of the ear pinna. After 16 hours, the animals were sacrificed and the injected area of the ear was separated and prepared for flow cytometry analysis.

Skin flow cytometry analysis

Mouse ears were split into the dorsal and ventral aspects, cut into small pieces, and incubated for 40 to 60 min at 37°C with constant shaking in RPMI 1640 medium containing DNase (100 μg/ml) and TM Liberase (62.5 μg/ml) or DNase (100 μg/ml) and collagenase D (2.5 mg/ml). Single-cell suspensions were generated using a GentleMACS dissociator (Miltenyi Biotec), and mechanical disruption was then performed using 50-μm cell strainers. Single-cell suspensions were kept on ice, dead cells were identified using the LIVE/DEAD Fixable Near-IR Dead Cell Stain Kit (Thermo Fisher), Fc receptors were blocked with the anti-CD16/32 antibody, and surface markers were stained with the appropriate fluorescent antibodies in FACS buffer (1% FBS, 5 mM EDTA, and 0.1% NaN_3). Intracellular staining was performed using the Cytofix/Cytoperm kit (BD Biosciences) as per the manufacturer's instructions. DCs were identified as CD45$^+$CD11c$^+$MHC-II$^+$CD64$^-$Ly6C$^-$, monocytes as CD45$^+$CD3$^-$CD19$^-$NK1.1$^-$Ly6C^{hi}Ly6G$^-$, and neutrophils as CD45$^+$CD3$^-$CD19$^-$NK1.1$^-$Ly6C^{lo}Ly6G$^+$.

CHS

CHS experiments were performed as described previously (*78*). Briefly, abdomens of 8- to 12-week-old C57BL/6J mice were shaved and sensitized the following day with 50 μl of 0.5% 2,4-dinitro-1-fluorobenzene (DNFB) in acetone or vehicle control. For experiments with lidocaine + QX314, 5 mg of QX314 and 5 mg of lidocaine in the form of 4% cream (Aspercreme) were applied to the shaved skin 4 hours before sensitization and in 24-hour intervals thereafter for the following 2 days. On day 5, mouse ears were challenged with 20 μl of 0.2% DNFB in acetone or vehicle control, and ear thickness was measured for the following 4 to 5 days. Antigen-specific ear swelling was calculated as DNFB-treated ear thickness minus control ear thickness. The experimenter performing ear-swelling measurements was blinded to mouse genotype and treatment group.

Statistical analysis

Statistical analyses were performed as described in figure legends. Student's *t* test was used for statistical comparisons of two experimental groups. If more than two experimental groups were present, one-way analysis of variance (ANOVA) with Tukey's multiple-comparisons test was used. For analyses that included two independent variables, two-way ANOVA with Tukey's multiple-comparisons test was used. All statistical analyses were performed in GraphPad Prism version 9.3.1 software.

REFERENCES AND NOTES

1. P. Baral, S. Udit, I. M. Chiu, Pain and immunity: Implications for host defence. *Nat. Rev. Immunol.* **19**, 433–447 (2019). doi: 10.1038/s41577-019-0147-2; pmid: 30874629
2. J. Ordovas-Montanes *et al.*, The regulation of immunological processes by peripheral neurons in homeostasis and disease. *Trends Immunol.* **36**, 578–604 (2015). doi: 10.1016/j.it.2015.08.007; pmid: 26431937
3. S. Huang *et al.*, Lymph nodes are innervated by a unique population of sensory neurons with immunomodulatory potential. *Cell* **184**, 441–459.e25 (2021). doi: 10.1016/j.cell.2020.11.028; pmid: 33333021
4. F. A. Pinho-Ribeiro, W. A. Verri Jr., I. M. Chiu, Nociceptor sensory neuron-immune interactions in pain and inflammation. *Trends Immunol.* **38**, 5–19 (2017). doi: 10.1016/j.it.2016.10.001; pmid: 27793571

5. C. J. Woolf, Q. Ma, Nociceptors—Noxious stimulus detectors. *Neuron* **55**, 353–364 (2007). doi: 10.1016/j.neuron.2007.07.016; pmid: 17678850
6. H. Veiga-Fernandes, D. Mucida, Neuro-immune interactions at barrier surfaces. *Cell* **165**, 801–811 (2016). doi: 10.1016/j.cell.2016.04.041; pmid: 27153494
7. M. Cabeza-Cabrerizo, A. Cardoso, C. M. Minutti, M. Pereira da Costa, C. Reis e Sousa, Dendritic cells revisited. *Annu. Rev. Immunol.* **39**, 131–166 (2021). doi: 10.1146/annurev-immunol-061020-053707; pmid: 33481643
8. S. W. Kashem *et al*., Nociceptive sensory fibers drive interleukin-23 production from CD301b+ dermal dendritic cells and drive protective cutaneous immunity. *Immunity* **43**, 515–526 (2015). doi: 10.1016/j.immuni.2015.08.016; pmid: 26377898
9. L. Riol-Blanco *et al*., Nociceptive sensory neurons drive interleukin-23-mediated psoriasiform skin inflammation. *Nature* **510**, 157–161 (2014). doi: 10.1038/nature13199; pmid: 24759321
10. C. Perner *et al*., Substance P release by sensory neurons triggers dendritic cell migration and initiates the type-2 immune response to allergens. *Immunity* **53**, 1063–1077.e7 (2020). doi: 10.1016/j.immuni.2020.10.001; pmid: 33098765
11. K. Tsujikawa *et al*., Hypertension and dysregulated proinflammatory cytokine production in receptor activity-modifying protein 1-deficient mice. *Proc. Natl. Acad. Sci. U.S.A.* **104**, 16702–16707 (2007). doi: 10.1073/pnas.0705974104; pmid: 17923674
12. S. Zelenay, C. Reis e Sousa, Adaptive immunity after cell death. *Trends Immunol.* **34**, 329–335 (2013). doi: 10.1016/j.it.2013.03.005; pmid: 23608152
13. A. M. Binshtok *et al*., Coapplication of lidocaine and the permanently charged sodium channel blocker QX-314 produces a long-lasting nociceptive blockade in rodents. *Anesthesiology* **111**, 127–137 (2009). doi: 10.1097/ALN.0b013e3181a915e7; pmid: 19512868
14. S. J. Gibson *et al*., Plasmacytoid dendritic cells produce cytokines and mature in response to the TLR7 agonists, imiquimod and resiquimod. *Cell. Immunol.* **218**, 74–86 (2002). doi: 10.1016/S0008-8749(02)00517-8; pmid: 12470615
15. H. Hemmi *et al*., Small anti-viral compounds activate immune cells via the TLR7 MyD88-dependent signaling pathway. *Nat. Immunol.* **3**, 196–200 (2002). doi: 10.1038/ni758; pmid: 11812998
16. T. Liu, Z. Z. Xu, C. K. Park, T. Berta, R. R. Ji, Toll-like receptor 7 mediates pruritus. *Nat. Neurosci.* **13**, 1460–1462 (2010). doi: 10.1038/nn.2683; pmid: 21037581
17. J. M. Lund *et al*., Recognition of single-stranded RNA viruses by Toll-like receptor 7. *Proc. Natl. Acad. Sci. U.S.A.* **101**, 5598–5603 (2004). doi: 10.1073/pnas.0400937101; pmid: 15034168
18. K. Esancy *et al*., A zebrafish and mouse model for selective pruritus via direct activation of TRPA1. *eLife* **7**, e32036 (2018). doi: 10.7554/eLife.32036; pmid: 29561265
19. J. J. Wei *et al*., Activation of TRPA1 nociceptor promotes systemic adult mammalian skin regeneration. *Sci. Immunol.* **5**, eaba5683 (2020). doi: 10.1126/sciimmunol.aba5683; pmid: 32859683
20. L. Deng, I. M. Chiu, Microbes and pain. *PLOS Pathog.* **17**, e1009398 (2021). doi: 10.1371/journal.ppat.1009398; pmid: 33793668
21. K. Maruyama *et al*., The ATP Transporter VNUT Mediates Induction of Dectin-1-Triggered Candida Nociception. *iScience* **6**, 306–318 (2018). doi: 10.1016/j.isci.2018.08.007; pmid: 30240621
22. V. Meseguer *et al*., TRPA1 channels mediate acute neurogenic inflammation and pain produced by bacterial endotoxins. *Nat. Commun.* **5**, 3125 (2014). doi: 10.1038/ncomms4125; pmid: 24445575
23. B. M. Assas, J. I. Pennock, J. A. Miyan, Calcitonin gene-related peptide is a key neurotransmitter in the neuro-immune axis. *Front. Neurosci.* **8**, 23 (2014). doi: 10.3389/fnins.2014.00023; pmid: 24592205
24. S. Suvas, Role of substance P neuropeptide in inflammation, wound healing, and tissue homeostasis. *J. Immunol.* **199**, 1543–1552 (2017). doi: 10.4049/jimmunol.1601751; pmid: 28827386
25. D. Ganea, M. Delgado, Vasoactive intestinal peptide (VIP) and pituitary adenylate cyclase-activating polypeptide (PACAP) as modulators of both innate and adaptive immunity. *Crit. Rev. Oral Biol. Med.* **13**, 229–237 (2002). doi: 10.1177/154411130201300303; pmid: 12090463
26. B. Lu *et al*., Abnormalities in monocyte recruitment and cytokine expression in monocyte chemoattractant protein 1-deficient mice. *J. Exp. Med.* **187**, 601–608 (1998). doi: 10.1084/jem.187.4.601; pmid: 9463410
27. X. J. Liu *et al*., TLR signaling adaptor protein MyD88 in primary sensory neurons contributes to persistent inflammatory and neuropathic pain and neuroinflammation. *Sci. Rep.* **6**, 28188 (2016). doi: 10.1038/srep28188; pmid: 27312666
28. C. L. Sokol, A. D. Luster, The chemokine system in innate immunity. *Cold Spring Harb. Perspect. Biol.* **7**, a016303 (2015). doi: 10.1101/cshperspect.a016303; pmid: 25635046
29. M. Gschwandtner, R. Derler, K. S. Midwood, More than just attractive: How CCL2 influences myeloid cell behavior beyond chemotaxis. *Front. Immunol.* **10**, 2759 (2019). doi: 10.3389/fimmu.2019.02759; pmid: 31921102
30. A. T. Satpathy *et al*., Zbtb46 expression distinguishes classical dendritic cells and their committed progenitors from other immune lineages. *J. Exp. Med.* **209**, 1135–1152 (2012). doi: 10.1084/jem.20120030; pmid: 22615127
31. M. J. Caterina *et al*., The capsaicin receptor: A heat-activated ion channel in the pain pathway. *Nature* **389**, 816–824 (1997). doi: 10.1038/39807; pmid: 9349813
32. A. M. Taylor *et al*., A microfluidic culture platform for CNS axonal injury, regeneration and transport. *Nat. Methods* **2**, 599–605 (2005). doi: 10.1038/nmeth777; pmid: 16094385
33. Y. L. Huang, A. S. Walker, E. W. Miller, A photostable silicon rhodamine platform for optical voltage sensing. *J. Am. Chem. Soc.* **137**, 10767–10776 (2015). doi: 10.1021/jacs.5b06644; pmid: 26237573
34. E. Shumilina, S. M. Huber, F. Lang, Ca2+ signaling in the regulation of dendritic cell functions. *Am. J. Physiol. Cell Physiol.* **300**, C1205–C1214 (2011). doi: 10.1152/ajpcell.00039.2011; pmid: 21451105
35. N. Matzner *et al*., Ion channels modulating mouse dendritic cell functions. *J. Immunol.* **181**, 6803–6809 (2008). doi: 10.4049/jimmunol.181.10.6803; pmid: 18981098
36. E. Huang, L. Showalter, S. Xu, B. J. Czerniecki, G. K. Koski, Calcium mobilizing treatment acts as a co-signal for TLR-mediated induction of Interleukin-12 (IL-12p70) secretion by murine bone marrow-derived dendritic cells. *Cell. Immunol.* **314**, 26–35 (2017). doi: 10.1016/j.cellimm.2017.01.010; pmid: 28190517
37. V. K. Mootha *et al*., PGC-1alpha-responsive genes involved in oxidative phosphorylation are coordinately downregulated in human diabetes. *Nat. Genet.* **34**, 267–273 (2003). doi: 10.1038/ng1180; pmid: 12808457
38. A. Subramanian *et al*., Gene set enrichment analysis: A knowledge-based approach for interpreting genome-wide expression profiles. *Proc. Natl. Acad. Sci. U.S.A.* **102**, 15545–15550 (2005). doi: 10.1073/pnas.0506580102; pmid: 16199517
39. A. Liberzon *et al*., The Molecular Signatures Database (MSigDB) hallmark gene set collection. *Cell Syst.* **1**, 417–425 (2015). doi: 10.1016/j.cels.2015.12.004; pmid: 26771021
40. S. K. Wculek, S. C. Khouili, E. Priego, I. Heras-Murillo, D. Sancho, Metabolic control of dendritic cell functions: Digesting information. *Front. Immunol.* **10**, 775 (2019). doi: 10.3389/fimmu.2019.00775; pmid: 31073300
41. L. Franchi, T. Eigenbrod, R. Muñoz-Planillo, G. Nuñez, The inflammasome: A caspase-1-activation platform that regulates immune responses and disease pathogenesis. *Nat. Immunol.* **10**, 241–247 (2009). doi: 10.1038/ni.1703; pmid: 19221555
42. T. S. P. Heng *et al*., The Immunological Genome Project: Networks of gene expression in immune cells. *Nat. Immunol.* **9**, 1091–1094 (2008). doi: 10.1038/ni1008-1091; pmid: 18800157
43. C. S. Walker, A. C. Conner, D. R. Poyner, D. L. Hay, Regulation of signal transduction by calcitonin gene-related peptide receptors. *Trends Pharmacol. Sci.* **31**, 476–483 (2010). doi: 10.1016/j.tips.2010.06.006; pmid: 20633935
44. Z. G. Goldsmith, D. N. Dhanasekaran, G protein regulation of MAPK networks. *Oncogene* **26**, 3122–3142 (2007). doi: 10.1038/sj.onc.1210407; pmid: 17496911
45. C. Perner, C. L. Sokol, Protocol for dissection and culture of murine dorsal root ganglia neurons to study neuropeptide release. *STAR Protoc.* **2**, 100333 (2021). doi: 10.1016/j.xpro.2021.100333; pmid: 33615276
46. F. A. Pinho-Ribeiro *et al*., Blocking neuronal signaling to immune cells treats streptococcal invasive infection. *Cell* **173**, 1083–1097.e22 (2018). doi: 10.1016/j.cell.2018.04.006; pmid: 29754819
47. S. Ständer *et al*., Expression of vanilloid receptor subtype 1 in cutaneous sensory nerve fibers, mast cells, and epithelial cells of appendage structures. *Exp. Dermatol.* **13**, 129–139 (2004). doi: 10.1111/j.0906-6705.2004.0178.x; pmid: 14987252
48. Z. Zasłona *et al*., The Induction of Pro-IL-1β by Lipopolysaccharide Requires Endogenous Prostaglandin E_2 Production. *J. Immunol.* **198**, 3558–3564 (2017). doi: 10.4049/jimmunol.1602072; pmid: 28298525
49. C. Shi *et al*., Bone marrow mesenchymal stem and progenitor cells induce monocyte emigration in response to circulating toll-like receptor ligands. *Immunity* **34**, 590–601 (2011). doi: 10.1016/j.immuni.2011.02.016; pmid: 21458307
50. A. D. Christensen, C. Haase, Immunological mechanisms of contact hypersensitivity in mice. *APMIS* **120**, 1–27 (2012). doi: 10.1111/j.1600-0463.2011.02832.x; pmid: 22151305
51. J. Filtjens *et al*., Nociceptive sensory neurons promote CD8 T cell responses to HSV-1 infection. *Nat. Commun.* **12**, 2936 (2021). doi: 10.1038/s41467-021-22841-6; pmid: 34006861
52. J. Liu, M. Chen, X. Wang, Calcitonin gene-related peptide inhibits lipopolysaccharide-induced interleukin-12 release from mouse peritoneal macrophages, mediated by the cAMP pathway. *Immunology* **101**, 61–67 (2000). doi: 10.1046/j.1365-2567.2000.00082.x; pmid: 11012754
53. I. M. Chiu *et al*., Bacteria activate sensory neurons that modulate pain and inflammation. *Nature* **501**, 52–57 (2013). doi: 10.1038/nature12479; pmid: 23965627
54. P. Baral *et al*., Nociceptor sensory neurons suppress neutrophil and γδ T cell responses in bacterial lung infections and lethal pneumonia. *Nat. Med.* **24**, 417–426 (2018). doi: 10.1038/nm.4501; pmid: 29505031
55. H. Nagashima *et al*., Neuropeptide CGRP limits group 2 innate lymphoid cell responses and constrains type 2 inflammation. *Immunity* **51**, 682–695.e6 (2019). doi: 10.1016/j.immuni.2019.06.009; pmid: 31353223
56. J. Helft *et al*., GM-CSF mouse bone marrow cultures comprise a heterogeneous population of CD11c(+)MHCII(+) macrophages and dendritic cells. *Immunity* **42**, 1197–1211 (2015). doi: 10.1016/j.immuni.2015.05.018; pmid: 26084029
57. M. Baliu-Piqué, G. Jusek, B. Holzmann, Neuroimmunological communication via CGRP promotes the development of a regulatory phenotype in TLR4-stimulated macrophages. *Eur. J. Immunol.* **44**, 3708–3716 (2014). doi: 10.1002/eji.201444553; pmid: 25316186
58. F. L. Liu *et al*., Interleukin (IL)-23 p19 expression induced by IL-1beta in human fibroblast-like synoviocytes with rheumatoid arthritis via active nuclear factor-kappaB and AP-1 dependent pathway. *Rheumatology (Oxford)* **46**, 1266–1273 (2007). doi: 10.1093/rheumatology/kem055; pmid: 17569750
59. A. Malecka *et al*., Stromal fibroblasts support dendritic cells to maintain IL-23/Th17 responses after exposure to ionizing radiation. *J. Leukoc. Biol.* **100**, 381–389 (2016). doi: 10.1189/jlb.3A1015-474R; pmid: 27049023
60. O. Chen, C. R. Donnelly, R. R. Ji, Regulation of pain by neuro-immune interactions between macrophages and nociceptor sensory neurons. *Curr. Opin. Neurobiol.* **62**, 17–25 (2020). doi: 10.1016/j.conb.2019.11.006; pmid: 31809997
61. J. Kupari *et al*., Single cell transcriptomics of primate sensory neurons identifies cell types associated with chronic pain. *Nat. Commun.* **12**, 1510 (2021). doi: 10.1038/s41467-021-21725-z; pmid: 33686078
62. D. Usoskin *et al*., Unbiased classification of sensory neuron types by large-scale single-cell RNA sequencing. *Nat. Neurosci.* **18**, 145–153 (2015). doi: 10.1038/nn.3881; pmid: 25420068
63. X. Wang, M. L. Veruki, N. V. Bukoreshtliev, E. Hartveit, H. H. Gerdes, Animal cells connected by nanotubes can be electrically coupled through interposed gap-junction channels. *Proc. Natl. Acad. Sci. U.S.A.* **107**, 17194–17199 (2010). doi: 10.1073/pnas.1006785107; pmid: 20855598
64. J. Ariazi *et al*., Tunneling nanotubes and gap junctions-their role in long-range intercellular communication during development, health, and disease conditions. *Front. Mol. Neurosci.* **10**, 333 (2017). doi: 10.3389/fnmol.2017.00333; pmid: 29089870
65. M. Krummen *et al*., Release of IL-12 by dendritic cells activated by TLR ligation is dependent on MyD88 signaling, whereas TRIF signaling is indispensable for TLR synergy. *J. Leukoc. Biol.* **88**, 189–199 (2010). doi: 10.1189/jlb.0408228; pmid: 20360404
66. M. Boes *et al*., T-cell engagement of dendritic cells rapidly rearranges MHC class II transport. *Nature* **418**, 983–988 (2002). doi: 10.1038/nature01004; pmid: 12198548
67. M. A. Nassar *et al*., Nociceptor-specific gene deletion reveals a major role for Nav1.7 (PN1) in acute and inflammatory pain. *Proc. Natl. Acad. Sci. U.S.A.* **101**, 12706–12711 (2004). doi: 10.1073/pnas.0404915101; pmid: 15314237
68. K. Brasel, T. De Smedt, J. L. Smith, C. R. Maliszewski, Generation of murine dendritic cells from flt3-ligand-supplemented bone marrow cultures. *Blood* **96**, 3029–3039 (2000). doi: 10.1182/blood.V96.9.3029; pmid: 11049981

69. J. Weischenfeldt, B. Porse, Bone marrow-derived macrophages (BMM): Isolation and applications. *CSH Protoc.* **2008**, pdb.prot5080 (2008). doi: 10.1101/pdb.prot5080; pmid: 21356739
70. S. Katzenell, J. R. Cabrera, B. J. North, D. A. Leib, Isolation, purification, and culture of primary murine sensory neurons. *Methods Mol. Biol.* **1656**, 229–251 (2017). doi: 10.1007/978-1-4939-7237-1_15; pmid: 28808974
71. T. Fath, Y. D. Ke, P. Gunning, J. Götz, L. M. Ittner, Primary support cultures of hippocampal and substantia nigra neurons. *Nat. Protoc.* **4**, 78–85 (2009). doi: 10.1038/nprot.2008.199; pmid: 19131959
72. J. Schindelin *et al*., Fiji: An open-source platform for biological-image analysis. *Nat. Methods* **9**, 676–682 (2012). doi: 10.1038/nmeth.2019; pmid: 22743772
73. B. C. Chen *et al*., Lattice light-sheet microscopy: Imaging molecules to embryos at high spatiotemporal resolution. *Science* **346**, 1257998 (2014). doi: 10.1126/science.1257998; pmid: 25342811
74. S. Picelli *et al*., Smart-seq2 for sensitive full-length transcriptome profiling in single cells. *Nat. Methods* **10**, 1096–1098 (2013). doi: 10.1038/nmeth.2639; pmid: 24056875
75. S. Picelli *et al*., Full-length RNA-seq from single cells using Smart-seq2. *Nat. Protoc.* **9**, 171–181 (2014). doi: 10.1038/nprot.2014.006; pmid: 24385147
76. S. X. Ge, E. W. Son, R. Yao, iDEP: An integrated web application for differential expression and pathway analysis of RNA-Seq data. *BMC Bioinformatics* **19**, 534 (2018). doi: 10.1186/s12859-018-2486-6; pmid: 30567491
77. H. Inoue, N. Nagata, Y. Koshihara, Participation of serotonin in capsaicin-induced mouse ear edema. *Jpn. J. Pharmacol.* **69**, 61–68 (1995). doi: 10.1254/jjp.69.61; pmid: 8847833
78. S. Paust *et al*., Critical role for the chemokine receptor CXCR6 in NK cell-mediated antigen-specific memory of haptens and viruses. *Nat. Immunol.* **11**, 1127–1135 (2010). doi: 10.1038/ni.1953; pmid: 20972432

ACKNOWLEDGMENTS

We thank H. Ploegh for sharing MHC-II eGFP mice; members of the von Andrian laboratory for helpful advice and discussions; and Harvard Medical School Electron Microscopy, Flow Cytometry, Microscopy Resources on the Northern Quad (MicRoN) and Cell Biology Microscopy facilities for technical assistance. Influenza PR8-GFP was generously provided by A. Garcia-Sastre at the Mount Sinai School of Medicine and the NIAID Centers of Excellence for Influenza Research and Surveillance program. *Streptococcus pneumoniae* was a kind gift from R. Malley at the Boston Children's Hospital and Harvard Medical School. **Funding:** This work was supported by the National Institutes of Health (grant AR068383 to U.H.v.A. and grant R01NS098088 to E.W.M.), a CRI Irvington postdoctoral fellowship (CRI2453 to P.H.), and the Howard Hughes Medical Institute (Gilliam Fellowship to G.O.). **Author contributions:** P.H. and U.H.v.A. conceived the study, interpreted the results, and wrote the manuscript. P.H. performed experiments and analyzed data. R.J.G. performed intradermal injections. I.B.M. generated BM chimeras and performed CHS experiments. Y.W. prepared cortical and hippocampal neuronal cultures. T.L. performed light sheet microscopy imaging. G.O. and E.W.M. generated the voltage-sensitive dye BeRST. **Competing interests:** U.H.v.A. is a paid consultant with financial interests in Avenge Bio, Beam Therapeutics, Bluesphere Bio, Curon, DNAlite, Gate Biosciences, Gentibio, Intergalactic, intrECate Biotherapeutics, Interon, Mallinckrodt Pharmaceuticals, Moderna, Monopteros Biotherapeutics, Morphic Therapeutics, Rubius, Selecta and SQZ. E.W.M. is an inventor on a patent describing BeRST-WO2017019908. The remaining authors declare no competing interests. **Data and materials availability:** RNA-seq data are available in the Gene Expression Omnibus (GEO) under GSE 217503, subseries GSE 217500 (data shown in Fig. 5) and GSE 217502 (data shown in Fig. 6C). All remaining data are available in the main text or the supplementary materials.

SUPPLEMENTARY MATERIALS

View/request a protocol for this paper from *Bio-protocol*.

Submitted 26 September 2021; resubmitted 12 August 2022
Accepted 17 February 2023
10.1126/science.abm5658

Multimodal control of dendritic cell functions by nociceptors

Pavel Han, Rodrigo J. Gonzalez, Irina B. Mazo, Yidi Wang, Talley Lambert, Gloria Ortiz, Evan W. Miller, and Ulrich H. von Andrian

Science, **379** (6639), eabm5658.
DOI: 10.1126/science.abm5658

Nociceptors and dendritic cells tango

Nociceptors are afferent neurons that transmit pain and itch sensations in response to noxious stimuli. Although they can influence dendritic cells (DCs), the specifics of nociceptor–DC cross-talk have been unclear. Han# *et al*. found that nociceptors can control DC functions in at least three ways that are context dependent (see the Perspective by Schraml). Nociceptors can attract DCs to tissues and regulate how long they stay there through the chemokine CCL21. When triggered, nociceptors can release the neuropeptide CGRP, which induces a “poised” DC gene program. Finally, nociceptors can trigger calcium ion flux and membrane depolarization in DCs, amplifying DC inflammatory responses through direct electrical coupling. This system allows the immune system to integrate pain with inflammatory and infectious signals in an exquisitely fine-tuned manner. —STS